Geochemical and mineralogical characterization and resource potential of the Namib Pb–Zn tailings (Erongo Region, Namibia)

by S. Lohmeier[1], D. Gallhofer[2], and B.G. Lottermoser[3]

Affiliation:
[1]Institute of Disposal Research, Department of Mineral Resources, and Institute of Mining Engineering, Department of Surface Mining and International Mining, Clausthal University of Technology, Clausthal-Zellerfeld, Germany
[2]Institute for Earth Sciences, University of Graz, Graz, Austria
[3]Institute of Mineral Resources Engineering, RWTH Aachen University, Aachen, Germany

Correspondence to:
S. Lohmeier

Email:
stephanie.lohmeier@tu-clausthal.de

Dates:
Received: 11 Mar. 2023
Revised: 31 May 2023
Accepted: 11 Jun. 2024
Published: August 2024

How to cite:
Lohmeier, S., Gallhofer, D., and Lottermoser, B.G. 2024. Geochemical and mineralogical characterization and resource potential of the Namib Pb–Zn tailings (Erongo Region, Namibia). *Journal of the Southern African Institute of Mining and Metallurgy*, vol. 124, no. 8. pp. 447–460

DOI ID:
http://dx.doi.org/10.17159/2411-9717/2724/2024

ORCID:
S. Lohmeier
http://orcid.org/0000-0003-2556-2096
D. Gallhofer
http://orcid.org/0000-0003-2139-7847
B.G. Lottermoser
http://orcid.org/0000-0002-8385-3898

Abstract

In Southern Africa, historic mining and mineral processing of base metal deposits have almost exclusively focussed on the extraction of major metals, leading to the loss of remaining valuable raw materials into tailings dumps and waste rock piles. At the Namib Pb–Zn mine (Erongo Region, Namibia), historic base metal tailings deposits are present as unreclaimed exposed waste piles. The tailings comprise silt- (fraction A: d_{50} = 25 to 48 µm) to sand-sized (fraction B: d_{50} = 86 to 185 µm; fraction C: d_{50} = 210 to 230 µm) material and contain major concentrations of base metals (Pb av. 1.15 mass%, Zn av. 3.20 mass%), S (av. 9.95 mass%), as well as lower values of other metals (Cu av. 490 µg/g, Cd av. 133 µg/g, Ag av. 22 µg/g), and critical elements like Sb (av. 14.7 µg/g) and In (14.3 µg/g). Former mineral processing only targeted the extraction of galena and sphalerite. As a consequence, qualitative mineralogical composition of the tailings is similar to that of the primary ore. Ca–Fe–Mg(–Mn) carbonates, quartz, micas, chlorite, minor graphite, magnetite, and rare parisite relate to the former host rock and gangue matrix, whereas Fe-rich sphalerite, galena, magnetite, pyrite with minor pyrrhotite, rare arsenopyrite, marcasite, cassiterite, and accessory scheelite are original constituents of the primary ore. Reprocessing of such a material would be challenging, but a mixed Pb–Zn concentrate enriched in Cd and Ag might be obtained. In future, possible reprocessing of Namib tailings and associated disposal of wastes into an appropriately designed repository would not only generate valuable metal commodities, but such activities would also eliminate a major metal pollution source from the local environment.

Keywords

Namib Pb–Zn deposit, tailings, base metals, resource, reprocessing

Introduction

Modern processing technologies allow a recovery of 80%–90% of ore, depending on grinding and the flotation agents used (Dold, 2010). However, many historic tailings dumps in Southern Africa originate from mining activities at the end of the 20th century or the colonial era or are even older, and have remained untouched for many years. In addition, about 75% of all worldwide mining projects close prematurely before ore is mined out, so valuable resources remain untouched or are even lost (Laurence, 2011). In times of increasing demand for resources (European Commission, 2010, 2017), such historic tailings dumps are of potential economic interest because the former ores were originally processed for particular metals, leaving other potential resources behind in the tailings (Lèbre et al., 2016; Lei et al., 2015). However, if such metalliferous tailings are left uncapped for extended periods, then they may become potential sources for metal contamination and thus likely hazards for human health and the environment (e.g., Festin et al., 2019; Harrison et al., 2010; Liakopoulos et al., 2010; Lupankwa et al., 2004), even in arid environments (Blight, 2007).

Nowadays, mining still focusses on the most profitable elements/metals, avoiding, at times, the extraction of other elements/metals as by-product(s), instead of using the whole potential of the ore as financial interests prevail (Mudd et al. 2017; West, 2020), even though full recovery of valuable components is often technically feasible and economic (Jahanshahi et al., 2007). In Namibia alone, there are more than 250 abandoned mine sites (Salom and Kivinen, 2019), of which many have potential to contain elements of economic interest. Pb–Zn ores, for example, have high potential for In, Cd, and Ga, which are elements of interest for modern technologies (Mudd et al., 2017; Werner et al., 2017).

The aim of this study is to document the general geochemical and mineralogical characteristics of the historic Namib Pb–Zn tailings at the Namib Pb–Zn mine site and to show the potential of these tailings as a

secondary metal resource (Figure 1). Hence, this study contributes to our understanding of the resource potential of historic tailings dumps with respect to relict metals that were not previously extracted.

Background

Mining site

The Namib Pb–Zn Mine is located about 25 km east of the town of Swakopmund and west of the Rössing Mountains in the Dorob National Park of Namibia's Erongo Region (22°31'17.53"S; 14°45'41.16"E; Figure 1A, B). Discovered during exploration activities between 1932 and 1934, underground mining for Pb, and later also for Zn and Ag, took place between 1968 to 1992 in the mine, formerly known as Deblin Mine or Namib Lead Mine, down to 210 m below surface (Snowden, 2014). Between 1992 and 1993, Iscor Namibia carried out some exploration activities. The mine site was then abandoned for several years, except for a short attempt to reprocess tailings for Zn by African Exploration in the mid-1990s (CCA, 2013; Snowden, 2014). However, recovery of Zn failed due to technical problems in suppressing flotation of pyrrhotite (Hahn et al., 2004; Snowden, 2014). In 2001, the tailings were granted to local geologists (CCA, 2013; Snowden, 2014), before Kalahari Mineral Limited carried out a detailed evaluation of the dumps via a reverse circulation drilling programme in 2008 (Snowden, 2014). At the same time, Kalahari Minerals Limited commenced drilling work on primary ore in 2007, before North River Resources took over the project in 2009, starting with cleaning the mine site and dewatering and surveying the underground workings as no remedial works were done prior to abandonment (CCA, 2013; Hahn et al., 2004; Snowden, 2014; Tenova Mining and Minerals, 2014). Since mid-2021, the Castlelake Group has held the largest stake of the Namib Pb–Zn mine, with North River Resources as minor stakeholder (NLZM, 2023). In 2014, a pre-feasibility study was published, followed by several optimization studies, outlining a remaining indicated primary JORC mineral resource of 710 000 t at a grade of 2.4% Pb, 7.0% Zn, and 50 g/t Ag related to four orebodies (South, Junction, North, and N20), plus an inferred resource of 409 000 t at a grade of 2.2% Pb, 6.0% Zn, and 38 g/t Ag and additional resources in close-by gossans (NLZM, 2023). Moreover, a preliminary JORC resource of 689 000 t at a grade of 32.1 g/t In (Snowden, 2014) or 0.9 Mt at a grade of 29 g/t In (Werner et al., 2017) was announced. Following limited mining and mineral processing in 2018 and 2019, the mine site remains under care and maintenance to this date.

Two tailings (slurry) dumps are located on site, having been produced during earlier mining and mineral processing activities, when ~100 000 t of Pb and Zn concentrate were produced from ~700 000 t of ore (CCA, 2013; Figure 1B-F). The former Ag production is estimated to exceed 1.1 Moz Ag. The older northern dump (~ 2.75 Mm^3; Hahn et al., 2004) traces back to the older mining activities, whereas the younger southern dump (~ 1.25 Mm^3; Hahn et al., 2004) is from the first reprocessing activities in the mid-1990s (CCA, 2013; Snowden, 2014). The remaining measured bulk tailings resource is estimated at 260 000 t at a grade of 0.3% Pb, 2.2% Zn, and 7.5 g/t Ag plus an additional indicated resource of 350 000 t at a grade of 0.3% Pb, 2.1% Zn, and 7.7 g/t Ag by NLZM (2023). However, Hahn et al. (2004) estimated the resource at 2.75 Mm^3 at a grade of 2.54% Zn, 0.21% Pb, and 7.0 g/t Ag (old dump) plus an additional 1.25 Mm^3 at a grade of 2.14% Zn, 0.15% Pb, and 7.9 g/t Ag (new dump). In the 2010s, Mintek proved recovery of Zn from the tailings to be uneconomic at that time (Snowden, 2014).

Slurries were largely preserved on-site due to the semi-arid climate in this part of the Namib desert after processing stopped. However, due to rare heavy rainfall events, as well as constant and, at times, strong winds resulting in wind erosion, the surrounding topsoils are covered, in particular in the downwind direction, to a certain degree by wind-blown material up to 8 km away from the site and up to 35 cm in thickness (CCA, 2013; Salom and Kivinen, 2019; Snowden, 2014). In addition, slurries are transported along drainage lines and contaminate stream sediments with Pb, Zn, As, and Cd (Hahn et al., 2004; SLR-EC, 2013). There are only ephemeral rivers in the surroundings: no acid mine drainage (AMD) has developed and no leaching of metals has taken place to date and is unlikely to develop, because AMD would be buffered by the carbonate host rock (SLR-EC, 2013). However, there is a distinct risk that seepage from the tailings dumps will influence groundwater quality through the addition of metals (SLR-EC, 2013). In future, covering/sealing of tailings dumps by marble waste rock is envisaged, which would reduce mobilization of remaining metals (e.g., CCA, 2013; Moreno and Neretnieks, 2006; Souissi et al., 2013).

Local geology and mineralization

At the Namib Pb–Zn Mine site, the Pb–Zn mineralization occurs within the calcitic 'mine marble', just above the contact with the underlying Arandis Formation (Basson et al., 2018; CCA, 2013). The mineralization is generally stratabound, but can cut across lithologies. Prolate and rhomb-shaped ore shoots dip between 45° and 90°, range in width between 2.5 and 13.6 m (av. 5.9 m), and have strike lengths of 9.6 to 91.2 m (av. 24.9 m; Basson et al., 2018; Snowden, 2014). The known minimum vertical extent of the ore shoots is > 210 m, corresponding to the current deepest mine level (Basson et al., 2018). Ore consists of sphalerite–galena–pyrrhotite–pyrite with locally abundant magnetite and fluorite (SLR-EC, 2013). In addition, Basson et al. (2018) reported locally anomalous In and Sn in the ore, without reference to the host mineral(s). Locally, gossans are characterized by ferruginous goethite- and hematite-bearing material with some occurrence of galena, cerussite, and smithsonite, which can extend down to 10 m depth below surface (Basson et al., 2018; Snowden, 2014). In general, oxidation extends down to ~ 16 m below surface (Snowden, 2014). Originally, the mineralization was defined as being of (remobilized) Mississippi Valley or sedimentary-exhalative type, evolved in the vicinity of a syn–rift growth fault (Basson et al., 2018; Frimmel and Miller, 2009; Snowden, 2014, and references therein), and was reinterpreted by mine geologists to be of intrusive-related carbonate replacement or manto type (CCA, 2013; SLR-EC, 2013). Based on structural investigations, Basson et al. (2018) described mineralization as remobilized and redeposited ore sequestered from a primary orebody in a tectonically activated stress field; however, mineralization has not yet been investigated in detail and is thus not fully understood.

The host rocks are mostly massive, white, coarse-grained marbles with intercalated fine-grained quartz–biotite–(feldspar–cordierite) schist and pegmatites (Badenhorst, 1987; CCA, 2013). Only very locally, weak lamination or colour-banding is developed (Lehtonen et al., 1996). Intercalations of calc-silicate layers and thin chert lenses or quartzite layers are rare (CCA, 2013; Lehtonen et al., 1996; Miller, 2008). Locally, 1–2 mm large graphite flakes (up to 5 vol.% of the mineral assemblage; Lehtonen et al., 1996), muscovite, and phlogopite can be abundant in the marble (Miller, 2008; MME, 1996), imparting a speckled appearance (Lehtonen et al., 1996). Fine-grained mylonite zones with and without graphite characterize the transition to the overlying Kuiseb schists (Miller, 2008).

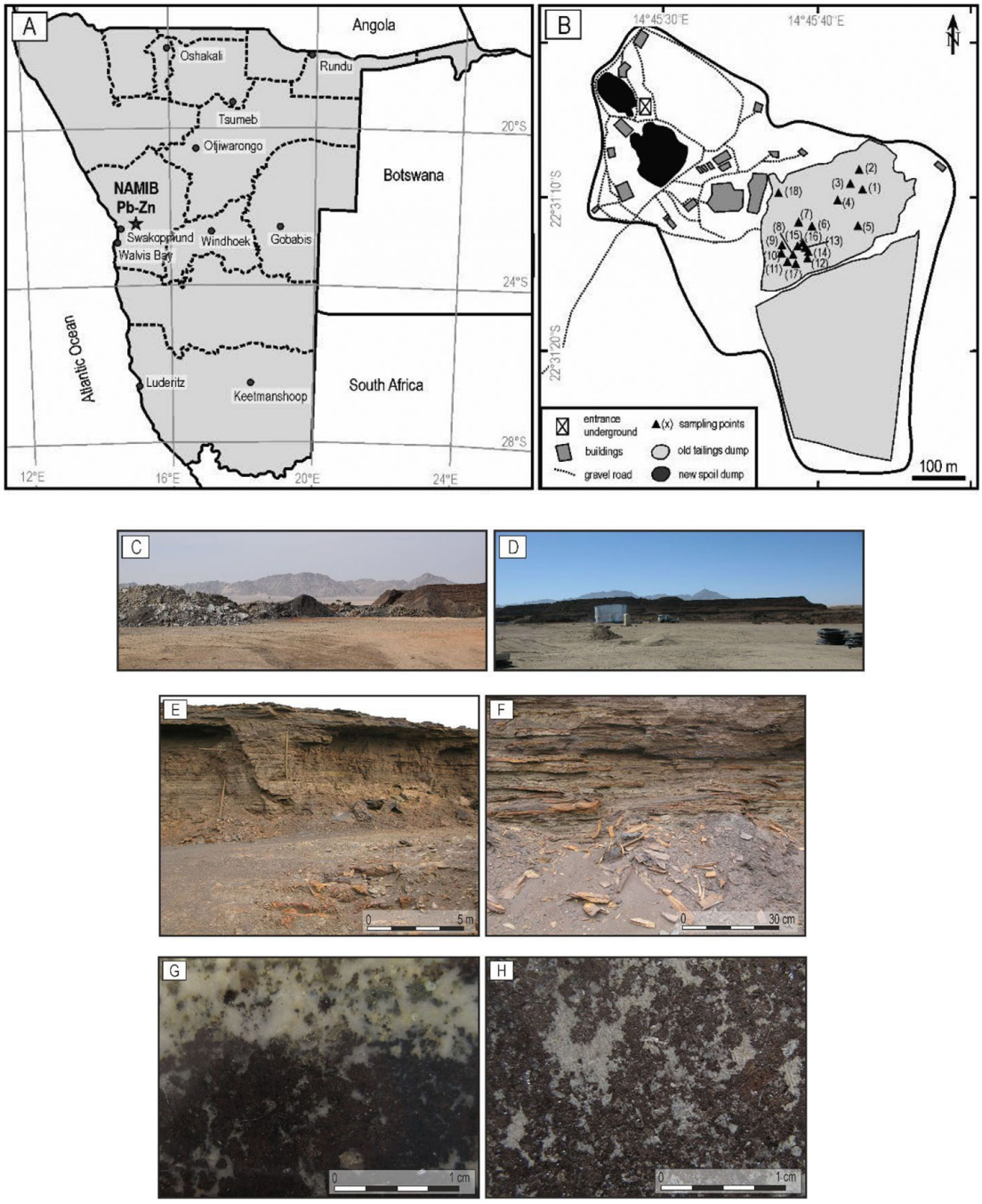

Figure 1—A: The Namib Pb–Zn deposit is located about 25 km east of the town of Swakopmund in Namibia's Erongo Region. B: Currently, the mine site comprises two smaller (new) spoil dumps and two large tailings dumps set onto a relatively flat underground. The older northern tailings dump, composed of solidified air-dried material, is distinctly higher than the younger southern tailings dump. Samples were taken from the older northern tailings dump because the reprocessing potential of this dump is assumed to be more promising. C–F: Photos showing the, higher, older northern tailings dump. Orange to brown colour variations of the solidified, air-dried material are apparent. The impression of centimeter-large rock pieces is misleading: the processing remains are largely composed of coarse silt to medium sand size ('powder size') material. 'Rock pieces' disintegrate during transport. Photographs taken by B.G. Lottermoser in 2018 and S. Lohmeier in 2019. G: Photograph showing primary Namib Pb–Zn ore composed of (visible) sphalerite (dark brown), galena (greyish), and pyrite intergrown with carbonate. H: Photograph showing sphalerite-dominated Namib Pb–Zn ore. G, H: Photographs taken by S. Lohmeier in 2022

Methodology

Sampling

Two large tailings dumps are located in the southern part of the Namib Pb–Zn mine site, SE of the main entrance to the underground mine (Figure 1B). Tailings range in grain size from clay to sand size ('powder size'). Larger hardened tailings blocks are present; however, these easily disintegrate to smaller pieces/grains (Figure 1E, F). In 2019, sampling focussed on the differently coloured tailings of the northern tailings dump to obtain different materials that represented different production cycles. Samples were collected along vertical profiles and directly from the surface of the tailings dump. In total, 18 tailings samples, each weighing ~ 5 kg, were taken. Two additional ore samples, representative of the principal ore mineralization according to the mine geologists, are from new stockpiles (Figure 1F, G).

Sample processing and analysis

Geochemical analysis

Tailings samples were air-dried and subsequently homogenized. A representative aliquot was milled to analytical fineness using a WC swing mill in the Department of Mineral Processing at RWTH Aachen University. Milled powders were sent to Australian Laboratory Services (ALS; Loughrea, Ireland) for X-ray fluorescence spectroscopy (XRF) of major elements (Al, Ca, Fe, K, Mg, Mn, Na, P, Si, Ti) for inductively coupled plasma mass spectrometry (ICP–MS) after HNO_3–HF–$HClO_4$ and HCl digestion for certain trace elements (Dy, Er, Eu, Gd, Ho, Nd, Pr, Sm, Tm), and for infrared (IR) spectroscopy of C and S. Loss on ignition (LOI) was determined by sintering at 1000°C. In addition, samples were analysed at SGS Bulgaria (Bor Laboratory, Serbia) by ICP–MS after HNO_3–HF–$HClO_4$ and HCl digestion for Ag, Al, As, Ba, Be, Bi, Ca, Cd, Ce, Co, Cr, Cs, Cu, Fe, Ga, Ge, Hf, In, K, La, Li, Lu, Mg, Mn, Mo, Nb, Na, Ni, P, Pb, Rb, Sb, Sc, Se, Sn, Sr, Ta, Tb, Te, Th, Ti, Tl, U, V, W, Y, Yb, Zn, and Zr. Samples having Ag > 10 µg/g, Pb > 10 000 µg/g, and/or Zn > 10 000 µg/g were reanalyzed by atomic emission spectroscopy (AES) using the same digestion approach. All sample packages included the analyses of duplicates and external and laboratory internal reference materials for quality control. Analytical data are given in Table I. X-ray diffraction (XRD) was performed on tailings samples and primary ore samples, using a X'Pert Pro (PANalytical) instrument with data collector and a X'Pert HighScore system equipped with a Co-LFF (Empyrian) tube and an automated divergence slit at the Institute of Disposal Research (IDR) at Clausthal University of Technology (TUC). Qualitative evaluation was carried out using the X'Pert HighScore software from PANalytical. Transmitted and reflected light microscopy was carried out on primary ore to correlate bulk geochemical data of tailings with mineralogical data.

Laser diffractometry and tailings density

Laser diffractometry in dry mode was applied after conventional wet sieving, screen washing, and laser diffractometry with hydro-dispersion failed due to clogging of sieves/screens and/or the analytical unit by the fines in a very short time. Moreover, laser diffractometry is the recommended method when a large quantity of particles is smaller than fine-sand size. All samples were dried and homogenized and lumps were gently comminuted before analysis. Particle size analysis was performed at the Institute of Mineral and Waste Processing, Recycling and Circular Economy Systems (TUC) using a HELOS H2387 Mastersizer instrument in dry mode. After initial test runs, the size range was set to 1 to 875 µm to include the whole particle size spectrum. No pre-screening was necessary. The instrument was run at 4 mbar external pressure and 44 mbar internal negative pressure as the dispersion method. Material charge (about 1.5 full spoon; ≤ 1 g) was by a vibration doser with a feed rate of 40% at a gap width of 7 mm. Analysis started when C_{opt} was ≥ 0.1% and stopped when C_{opt} was ≤ 0.1% for 2 s. All runs were repeated three times. Evaluation was done using the PAQXOS 4.3 software of HELOS. It should be noted that results of sand-sized material are comparable with those obtained by the classical sieving-pipette method, but deviations for clay-sized material may occur (e.g., Beuselinck et al., 1998; Konert and Vandenberghe, 1997; Miller and Schaetzl, 2011). It was intended to give a general overview of the Namib Pb–Zn tailings so that data collected by laser diffraction are of sufficient quality. However, a certain bias by platy particles, such as graphite flakes and micas, cannot be excluded.

The density of the tailings material was semi-quantitatively determined in two different ways. These approaches were chosen because the material loosened on transport, losing its original compact state. Thus, the bulk density of the tailings can be only approximately determined after liberation of the material from the tailings pile and transport. The first approach was by filling an 80 mL flask with the loosened material and subsequent weighing the material to determine the bulk or powder density without any additional compaction. The gross density was then calculated under consideration of the decompaction factor, which was set here to 0.6, equivalent to material of medium density (Dachroth, 2017; DIN 18300). The second approach was by calculating the density from bulk geochemical data and mineral proportions.

Results

Primary ore

Primary ore mineralogy

Primary Namib Pb–Zn ore is characterized by visible massive dark to very dark coloured sphalerite and galena (Figures 1G, F, 2A) set into a Ca–Mg–Fe(–Mn) carbonate matrix. Microscopy reveals the presence of minor micas, including phlogopite, biotite, and muscovite, as well as quartz, zircon, apatite, and graphite flakes (Figure 2B) as part of the matrix. Pyrite is the most abundant minor sulfide mineral and occurs mostly as small patches enclosed in sphalerite or in small fissures and fractures crosscutting sphalerite (Figure 2C, D) and overgrowing micas. The presence of rare relict anhedral to partially subhedral marcasite enclosed in pyrite reveals that the paragenesis galena–sphalerite–pyrite is post-marcasite. At least two different pyrite generations could be identified using microscopy. The younger pyrite generation comprises fine-crystalline 'porous' pyrite crystals, whereas the older pyrite generation is characterized by anhedral to partly subhedral pyrite. Marcasite is consistently associated with 'porous'

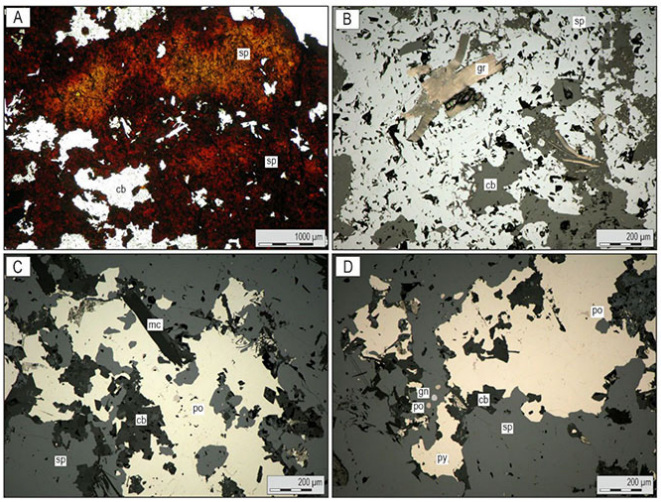

Figure 2—A–D: Photomicrographs of primary Namib Pb–Zn ore. A: Massive sphalerite set into carbonate matrix. B: Graphite flakes in massive sphalerite with carbonate matrix. C: Small pyrrhotite crystals enclosed in massive pyrite. Pyrite–pyrrhotite are enclosed in massive sphalerite with carbonate matrix. D: Pyrrhotite enclosed in massive pyrite and as small rounded inclusions, together with galena, in massive sphalerite. A: Transmitted light, straight polars; B–D: Reflected light. Abbreviations: cb = Ca–Mg–Fe(–Mn) carbonate; gn = galena; gr = graphite; mc = mica; po = pyrrhotite; py = pyrite; sp = sphalerite

Table I

Bulk rock analytical results for Namib Pb–Zn tailings. Values of Ge are < 5 µg/g, of Se mostly < 2 µg/g, of Te mostly < 0.05 µg/g. Primary ore samples were only analyzed by ICP–MS. Tailings analyses were analyzed by (1) XRF, (2) ICP-MS, (3) AES, (4) IR, and (5) Loss on ignition

Analytes	Si	Ti	Ti	Al	Al	Fe	Fe	Mn	Mn	Mg	Mg	Ca	Ca	Na	Na	K	K
Unit	mass%	mass%	mass%	[mass%	mass%	mass%	mass%	mass%	mass%	mass%	mass%	mass%	mass%	mass%	mass%	mass%	mass%
Method	(1)	(2)	(1)	(2)	(1)	(2)	(1)	(2)	(1)	(2)	(1)	(2)	(1)	(2)	(1)	(2)	(1)
NBT-1	2.54	0.03	0.05	0.45	0.56	26.11	30.98	> 1.00	1.29	0.15	0.25	10.97	8.79	0.06	0.08	0.30	0.32
NBT-2	5.42	0.04	0.07	0.92	1.11	17.50	19.56	> 1.00	1.92	0.24	0.36	> 15.00	15.72	0.18	0.17	0.60	0.65
NBT-3	5.24	0.04	0.05	1.05	1.12	17.30	17.20	> 1.00	1.95	0.33	0.45	> 15.00	17.01	0.34	0.30	0.68	0.65
NBT-4	6.87	0.06	0.08	1.07	1.34	19.84	22.51	> 1.00	1.53	0.25	0.40	> 15.00	12.08	0.23	0.23	0.68	0.77
NBT-5	5.59	0.05	0.07	0.94	1.15	19.52	21.58	> 1.00	1.93	0.27	0.42	> 15.00	13.69	0.18	0.17	0.63	0.66
NBT-6	3.66	0.04	0.05	0.80	0.97	16.67	18.55	> 1.00	2.81	0.60	0.94	> 15.00	15.51	1.08	1.14	0.58	0.62
NBT-7	4.10	0.05	0.06	1.07	1.21	16.30	17.41	> 1.00	2.39	1.24	1.31	> 15.00	15.15	1.82	1.83	0.70	0.72
NBT-8	5.46	0.04	0.07	1.28	1.43	16.61	17.81	> 1.00	1.66	0.31	0.44	> 15.00	17.22	0.13	0.12	0.75	0.76
NBT-9	3.64	0.03	0.07	0.69	0.85	16.78	20.67	> 1.00	1.43	0.25	0.42	14.90	11.47	0.24	< 0.01	0.43	0.49
NBT-10	4.66	0.03	0.06	1.28	1.57	14.33	16.67	> 1.00	0.82	0.55	0.88	13.08	9.83	3.14	3.41	0.84	0.94
NBT-11	4.31	0.04	0.05	1.22	1.27	17.16	16.31	> 1.00	1.25	0.39	0.52	> 15.00	14.94	0.88	0.82	0.74	0.70
NBT-12	3.06	0.03	0.05	0.71	0.79	18.36	19.56	> 1.00	1.92	0.33	0.49	> 15.00	14.08	0.33	0.24	0.44	0.44
NBT-13	5.07	0.05	0.07	1.13	1.25	19.08	20.17	> 1.00	1.56	0.27	0.40	> 15.00	15.01	0.14	0.12	0.67	0.66
NBT-14	3.30	0.03	0.05	0.87	0.93	15.11	15.85	> 1.00	2.29	0.41	0.61	> 15.00	18.87	0.39	0.36	0.55	0.52
NBT-15	3.33	0.03	0.04	0.88	0.91	15.49	15.46	> 1.00	2.28	0.44	0.60	> 15.00	18.65	0.60	0.53	0.56	0.51
NBT-16	3.44	0.03	0.05	0.68	0.81	17.78	21.06	> 1.00	1.62	0.28	0.47	> 15.00	11.76	0.20	0.05	0.43	0.45
NBT-17	3.22	0.03	0.05	0.75	0.87	18.67	20.12	> 1.00	1.73	0.33	0.50	> 15.00	12.90	0.31	0.21	0.46	0.46
NBT-18	3.60	0.04	0.07	0.73	0.87	20.64	24.55	> 1.00	1.39	0.20	0.33	13.02	9.51	0.17	0.04	0.44	0.47
NAM-1		0.01		0.87		10.04		0.50		0.15		3.88		< 0.01		0.50	
NAM-2		0.02		0.88		10.01		0.48		0.15		5.72		< 0.01		0.51	

Analytes	P	P	S	C	LOI	Ag	As	Ba	Be	Bi	Cd	Ce	Co	Cr	Cs	Cu	Dy
Unit	mass%	mass%	mass%	mass%	mass%	µg/g	µg/g	µg/g	µg/g	µg/g	µg/g	µg/g	µg/g	µg/g	µg/g	µg/g	µg/g
Method	(2)	(1)	(4)	(4)	(5)	(2) (3)	(2)	(2)	(2)	(2)	(2)	(2)	(2)	(2)	(2)	(2) (3)	(2)
NBT-1	0.02	0.03	13.80	1.31	19.00	12	587	37	0.3	45.7	43	25	6.1	9	14.0	124	0.93
NBT-2	0.03	0.02	7.51	3.33	13.53	6.53	198	88	0.4	5.56	39	30	6.4	13	11.2	124	1.33
NBT-3	0.03	0.03	7.15	4.55	16.06	6.31	92.5	97	0.4	3.62	62	27	19.1	13	7.2	151	1.31
NBT-4	0.03	0.03	8.52	3.19	10.05	6.55	100	125	0.4	4.06	39	26	7.1	13	5.3	111	1.69
NBT-5	0.03	0.03	7.62	3.85	12.70	6.26	130	92	0.4	9.89	32	31	9.6	12	10.8	108	1.63
NBT-6	0.02	0.02	6.74	5.01	15.95	8.78	170	59	0.5	10.8	83	36	15.0	12	28.7	650	1.89
NBT-7	0.03	0.03	6.86	4.57	16.24	7.71	109	72	0.4	7.44	90	37	27.0	15	24.0	525	1.87
NBT-8	0.03	0.03	8.51	4.94	8.74	8.30	149	75	0.4	3.59	62	46	5.6	15	5.0	229	1.96
NBT-9	0.02	0.03	14.65	3.34	13.01	83	133	57	0.3	7.88	399	25	24.3	12	4.2	585	1.15
NBT-10	0.03	0.03	12.20	1.53	19.91	17	231	61	0.4	12.3	88	34	4.7	19	6.1	252	1.19
NBT-11	0.03	0.03	9.96	4.59	9.89	10	85.8	68	0.4	3.02	73	39	12.6	22	3.4	240	1.65
NBT-12	0.02	0.02	11.15	5.51	9.37	31	156	63	0.3	9.67	262	29	18.5	15	8.6	1 479	1.27
NBT-13	0.03	0.03	10.80	3.54	6.72	12	109	77	0.3	6.04	86	33	7.8	15	5.6	280	1.55
NBT-14	0.02	0.02	6.71	7.41	16.16	15	105	75	0.3	4.07	126	32	6.0	16	11.5	1 340	1.48
NBT-15	0.02	0.02	6.51	7.10	16.66	15	110	77	0.3	3.80	130	30	6.2	15	10.0	850	1.44
NBT-16	0.02	0.03	13.60	3.86	12.08	53	174	57	0.2	7.35	268	26	14.9	11	5.5	805	1.20
NBT-17	0.02	0.03	13.40	4.68	12.15	52	192	54	0.3	6.15	269	34	18.6	13	6.4	658	1.83
NBT-18	0.02	0.03	13.45	2.61	12.54	52	404	53	0.2	14.6	243	24	8.0	12	6.1	301	1.20
NAM-1	0.04					16	37.6	29	0.2	0.07	978	50	6.6	21	0.7	111	
NAM-2	0.04					21	44.6	35	0.2	0.08	1042	74	4.8	23	0.7	109	

Analytes	Er	Eu	Ga	Gd	Hf	Ho	In	La	Li	Lu	Mo	Nb	Nd	Ni	Pb	Pr	Rb
Unit	µg/g	µg/g	µg/g	µg/g	µg/g	µg/g	µg/g	µg/g	µg/g	µg/g	µg/g	µg/g	µg/g	µg/g	µg/g	µg/g	µg/g
Method	(2)	(2)	(2)	(2)	(2)	(2)	(2)	(2)	(2)	(2)	(2)	(2)	(2)	(2)	(2) (3)	(2)	(2)
NBT-1	0.36	1.49	3.9	0.86	0.24	0.09	5.39	16.7	8.7	0.06	1.61	1.2	9.3	10.3	4 277	2.63	43.3
NBT-2	0.84	2.61	5.3	1.91	0.22	0.18	4.34	19.3	11.4	0.12	1.43	1.5	13.3	12.4	1 749	3.67	55.6
NBT-3	0.75	2.05	5.7	1.85	0.31	0.14	5.16	17.8	13.5	0.11	1.23	1.5	12.0	11.1	1 624	3.28	53.7
NBT-4	0.97	1.72	5.5	1.89	0.26	0.24	4.59	16.0	8.7	0.08	2.34	2.3	11.5	11.6	2 058	3.34	47.8
NBT-5	0.76	2.30	5.6	2.10	0.18	0.25	4.08	19.9	11.4	0.08	1.33	1.8	13.8	10.3	1 643	3.85	56.8
NBT-6	0.81	3.15	6.2	1.77	0.25	0.27	9.47	23.8	22.4	0.09	1.15	1.3	15.1	10.4	2 013	4.02	91.7
NBT-7	1.09	3.10	7.7	2.05	0.19	0.37	8.97	24.4	28.2	0.11	2.46	1.4	13.6	11.0	1 786	4.14	93.2
NBT-8	1.02	3.07	8.4	2.46	0.23	0.38	8.20	30.8	8.7	0.11	1.01	1.4	18.4	10.5	2 556	5.47	61.9
NBT-9	0.74	1.79	6.3	1.61	0.15	0.22	40.0	15.8	6.5	0.08	0.83	1.1	9.7	9.7	56 900	2.77	35.7
NBT-10	0.70	1.82	10.6	1.72	0.15	0.21	13.9	21.9	14.9	0.06	0.68	0.9	13.9	9.2	5 191	4.07	70.8
NBT-11	0.84	2.27	9.1	2.19	0.25	0.31	8.69	25.5	10.0	0.09	0.95	1.2	15.7	12.2	3 180	4.65	62.3
NBT-12	0.68	2.09	6.3	1.60	0.20	0.25	23.6	19.1	9.0	0.08	1.52	1.1	10.5	12.8	17 600	3.21	42.4
NBT-13	0.80	2.12	7.9	2.04	0.29	0.31	12.1	21.4	9.0	0.10	0.95	1.5	13.5	11.1	4 208	3.70	55.3
NBT-14	0.75	2.39	6.6	1.82	0.27	0.27	11.8	21.1	11.3	0.09	1.46	1.1	11.9	11.7	7 575	3.55	51.5
NBT-15	0.79	2.40	6.7	1.77	0.18	0.28	12.2	20.4	11.8	0.10	1.48	0.9	12.1	11.8	6 241	3.58	50.6
NBT-16	0.69	1.91	5.7	1.59	0.18	0.24	25.6	17.4	6.7	0.09	0.83	1.0	10.6	9.6	28 900	3.12	38.6
NBT-17	0.91	2.45	6.4	2.15	0.11	0.33	24.0	22.3	7.5	0.10	0.92	0.8	13.6	10.3	29 800	3.98	44.3
NBT-18	0.57	1.58	5.9	1.35	0.25	0.21	36.1	15.9	7.8	0.06	0.74	1.4	9.5	9.6	30 100	2.66	38.2
NAM-1			11.0		0.23		85.8	37.3	2.3	0.06	0.42	1.7		5.4	9 069		36.6
NAM-2			11.1		0.21		85.5	51.8	2.5	0.09	0.48	2.2		5.4	9 300		36.7

Analytes	Sb	Sc	Sm	Sn	Sr	Ta	Tb	Th	Tl	Tm	U	V	W	Y	Yb	Zn	Zr
Unit	µg/g	µg/g	µg/g	µg/g	µg/g	µg/g	µg/g	µg/g	µg/g	µg/g	µg/g	µg/g	µg/g	µg/g	µg/g	µg/g	µg/g
Method	(2)	(2)	(2)	(2)	(2)	(2)	(2)	(2)	(2)	(2)	(2)	(2)	(2)	(2)	(2)	(2) (3)	(2)
NBT-1	9.27	1.2	1.19	15.0	132	0.2	0.18	1.9	1.70	0.03	1.5	3.7	66	4.3	0.3	12 000	5.1
NBT-2	4.84	1.8	2.81	14.6	322	0.5	0.28	2.0	1.51	0.08	1.9	9.5	34	7.3	0.5	12 400	5.4
NBT-3	4.80	1.8	2.10	17.0	457	1.2	0.30	1.6	1.09	0.05	2.1	10.7	64	7.3	0.7	12 800	7.1
NBT-4	4.90	1.8	2.12	13.3	276	0.6	0.26	4.7	0.91	0.14	2.3	10.4	43	6.8	0.6	10 500	8.1
NBT-5	4.53	1.7	2.44	16.1	291	0.9	0.25	2.0	1.36	0.06	1.9	9.1	64	6.9	0.6	8 906	5.5
NBT-6	5.01	1.9	2.41	18.1	301	0.3	0.31	1.6	3.36	0.08	1.5	8.8	44	7.6	0.6	17 700	5.8
NBT-7	5.71	2.2	2.59	32.2	314	0.5	0.34	2.4	3.14	0.13	2.1	13.1	65	8.2	0.8	15 300	6.5
NBT-8	4.73	2.6	3.41	26.1	350	0.4	0.38	2.8	1.22	0.11	2.2	16.3	49	9.0	0.8	15 700	6.3
NBT-9	43.7	1.4	1.86	40.2	227	0.6	0.22	2.2	0.98	0.07	1.9	7.4	60	6.0	0.5	95 700	4.2
NBT-10	8.04	2.1	2.47	30.1	269	0.2	0.23	1.7	1.44	0.06	1.9	17.7	31	5.1	0.5	13 100	4.6
NBT-11	6.55	2.7	2.92	31.3	386	0.8	0.29	2.0	0.99	0.09	2.1	17.1	58	7.6	0.7	16 400	5.8
NBT-12	22.3	1.4	1.94	31.8	321	0.8	0.20	1.6	1.24	0.09	1.9	7.3	56	6.2	0.6	59 600	4.3
NBT-13	7.79	2.4	2.26	25.4	361	0.7	0.28	2.4	1.00	0.11	2.3	14.0	49	7.4	0.6	20 500	6.2
NBT-14	17.5	1.9	2.06	26.0	451	0.4	0.30	1.8	1.47	0.07	2.0	11.4	42	7.4	0.6	30 800	4.2
NBT-15	12.7	1.8	2.38	23.9	482	0.4	0.27	1.5	1.30	0.07	2.1	9.6	39	7.4	0.7	30 800	3.9
NBT-16	32.7	1.4	2.04	29.4	232	0.4	0.23	1.6	1.02	0.06	1.9	7.1	34	5.7	0.5	68 300	5.1
NBT-17	36.7	1.7	2.52	34.2	213	0.4	0.33	2.1	1.13	0.08	2.1	7.6	37	7.9	0.7	65 500	4.1
NBT-18	32.9	1.6	1.73	25.4	197	0.5	0.21	1.6	1.16	0.07	1.6	9.5	49	4.9	0.4	70 300	5.4
NAM-1	7.71	1.1		22.4	17.6	0.1	0.25	1.0	2.54		1.7	8.1	8.0	4.9	0.4	330 600	5.1
NAM-2	7.70	1.4		25.5	29.4	0.1	0.37	1.2	2.31		1.6	6.4	7.3	6.5	0.5	338 000	4.8

pyrite crystals, suggesting that the formation of marcasite was subsequently followed by transformation of the metastable marcasite polymorph into the more stable pyrite polymorph. In addition, the ore paragenesis comprises minor anhedral pyrrhotite that is mostly enclosed in massive pyrite, but can occur also as discrete minerals in sphalerite (Figure 2C–D). Arsenopyrite, cassiterite, and parisite are rare. Scheelite is an accessory. Cassiterite and scheelite are either (partly) overgrown by galena and/or pyrite or occur in the carbonate matrix, so they are pre-galena–sphalerite–pyrite. Parisite locally overgrows cassiterite and is enclosed in pyrite, identifying parisite as post-cassiterite and pre-galena–sphalerite(–pyrite). The temporal relations of arsenopyrite cannot be constrained because arsenopyrite is only observed as inclusions in massive sphalerite. No gypsum and no goethite are observed in massive primary Namib Pb–Zn ore.

Primary ore geochemistry and bulk enrichment

The two primary ore samples have quite similar geochemical composition. Based on ICP–MS and AES data, Zn (33.06 and 33.80 mass%), Fe (10.01 and 10.04 mass%), and Ca (3.88 and 5.72 mass%) constitute by far the largest proportions of bulk samples (Figure 3A; Table I). Relatively high contents are also present for Pb (0.91 and 0.93 mass%), Al (0.87 and 0.88 mass%), K (0.50 and 0.51 mass%), and Mn (0.48 and 0.49 mass%), whereas Mg (both: 0.15 mass%) and Cd (both: 0.10 mass%) concentrations are somewhat minor. All other elements have concentrations of ≤ 400 µg/g. Average P (~ 400 µg/g), Ti (~ 150 µg/g), and Cu (~ 110 µg/g) concentrations are in the range of 100 to 400 µg/g, while In (~ 86 µg/g), Ce (~ 62 µg/g), La (~ 45 µg/g), Rb (~ 37 µg/g), Ba (~ 32 µg/g), Sn (~ 24 µg/g), Sr (~ 24 µg/g), Nd (~ 23 µg/g), Cr (~ 22 µg/g), Ag (~ 19 µg/g), As (~ 19 µg/g), and Ga (~ 11 µg/g) average contents are between 10 and 90 µg/g. In contrast Sb (~ 7.7 µg/g), W (~ 7.7 µg/g), V (~ 7.3 µg/g), Pr (~ 6.3 µg/g), Co (~ 5.7 µg/g), Y (~ 5.7 µg/g), Ni (~ 5.4 µg/g), Zr (~ 5.0 µg/g), Eu (~ 4.4 µg/g), Sm (~ 3.3 µg/g), Gd (~ 2.8 µg/g), Tl (~ 2.4 µg/g), Li (~ 2.4 µg/g), Nb (~ 2.0 µg/g), U (~ 1.7 µg/g), Dy (~ 1.3 µg/g), Sc (~ 1.3 µg/g), and Th (~1 .2 µg/g) averages are between 8 and 1 µg/g, and Cs, Er, Mo, Yb, Tb, Hf, Ho, Be, Bi, Lu, Tm, and Ta averages are < 1 µg/g. By far the most enriched element in primary ore, compared with bulk crustal abundance, is Cd, with an enrichment of 12 600×. Additionally, Zn (4643×), In (1646×), Pb (835×), and Ag (330×) are strongly enriched and thus the same elements as in tailings material (see below). A distinct enrichment is also seen in Sb (38×), As (16×), and Sn (14×), while W (8×), Mn (6×), and Tl (5×) show a very slight enrichment compared with bulk crustal abundance. All other elements are not enriched or enrichment is ≤ 4×.

Tailings

Particle size and tailings density

The particle-size distribution curves of Namib Pb–Zn tailings cover the size spectrum from clay to medium sand, as is typical for fine-grained tailings (average data for three runs are provided in Table II). Three different particle fractions can be distinguished by median/mean values and curve shapes (Figure 4). Fraction A (six samples) comprises tailings with a dominant silt component, whereas Fraction B (eight samples) and Fraction C (three samples) comprise samples with a prevailing sand component. Fraction B is thereby largely composed of fine sand-sized particles while also having a relatively high silt component, whereas Fraction C has a quite narrow particle range with most particles in the medium sand-size range.

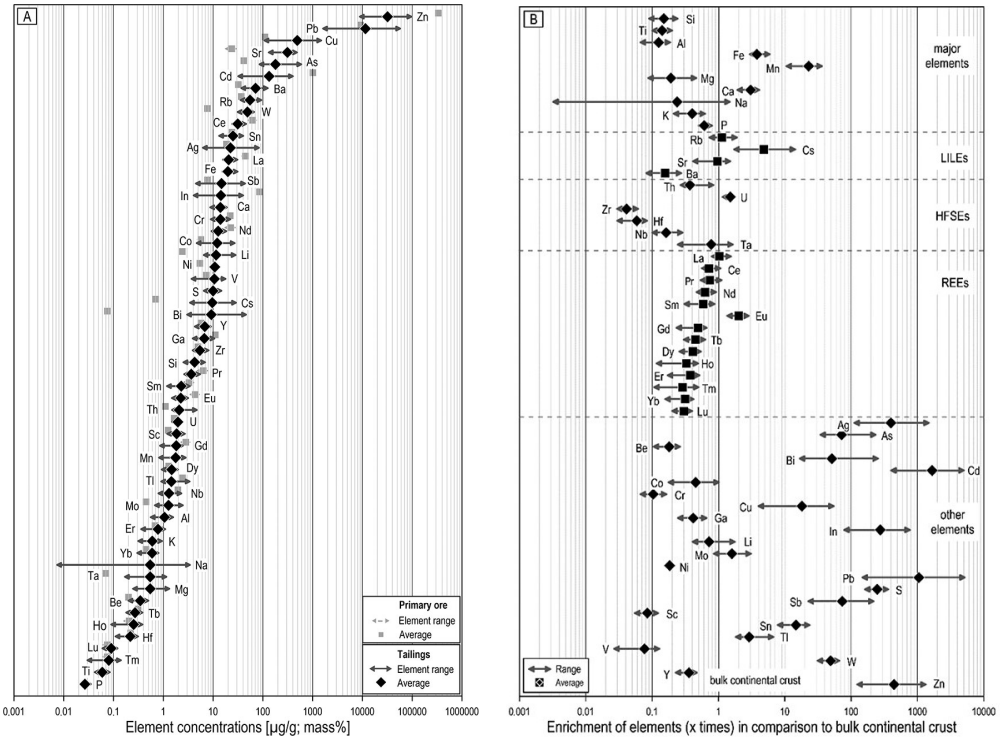

Figure 3—A: Element ranges of tailings and primary ore samples. Major elements are in mass%, whereas minor and trace elements are in µg/g. B: Enrichment of elements of Namib Pb–Zn tailings in comparison with bulk continental crust (data from Rudnick and Gao, 2003). Elements are assigned to major elements, large-ion lithophile elements (LILE), high-field strength elements (HFS), rare earth elements (REE; including here only the lanthanides), and other elements. There is probably some bias concerning W because a WC mill was used during sample preparation. A, B: For major elements XRF data was used. Sulfur values are by IR. ICP-MS data was used for minor and trace elements

Table II

Results of laser diffractometry of Namib Pb–Zn tailings (averages of three runs per sample), particle size statistical parameters based on sieving curves, and bulk density. (1) Mass of 80 mL flask (g); (2) powder density by weighing (g/cm³); (3) gross density by weighing in (g/cm³); (4) density calculated from geochemical data (g/cm³)

Grain size [µm]	NBT1 [%]	NBT2 [%]	NBT3 [%]	NBT4 [%]	NBT5 [%]	NBT6 [%]	NBT7 [%]	NBT8 [%]	NBT9 [%]	NBT10 [%]	NBT11 [%]	NBT12 [%]	NBT13 [%]	NBT14 [%]	NBT15 [%]	NBT16 [%]	NBT17 [%]	NBT18 [%]
≤ 1.0	0.0	0.0	0.0	0.0	0.0	0.0	0.0	0.0	0.0	0.0	0.0	0.0	0.0	0.0	0.0	0.0	0.0	0.0
≤ 4.5	6.8	1.8	1.5	3.2	1.7	10.8	9.0	10.8	7.8	6.2	13.8	14.2	10.6	18.8	15.9	7.3	9.7	4.2
≤ 5.5	8.0	2.1	1.8	3.7	2.0	12.9	10.8	12.8	9.2	7.5	16.2	16.7	12.5	22.0	18.6	8.6	11.4	4.9
≤ 6.5	9.2	2.4	2.0	4.1	2.2	14.8	12.5	14.5	10.6	8.8	18.4	18.9	14.2	24.7	20.9	9.9	13.0	5.6
≤ 7.5	10.2	2.6	2.2	4.6	2.4	16.5	14.1	16.1	11.8	10.0	20.4	21.0	15.7	27.2	23.2	11.0	14.5	6.2
≤ 9.0	11.6	3.0	2.5	5.1	2.7	19.0	16.3	18.3	13.5	11.8	23.0	23.6	17.8	30.4	25.8	12.6	16.5	6.9
≤ 11.0	13.3	3.4	2.8	5.8	3.0	22.0	19.0	20.9	15.5	14.0	26.2	26.8	20.2	34.0	29.0	14.4	18.8	7.8
≤ 13.0	14.8	3.7	3.1	6.3	3.2	24.7	21.5	23.2	17.3	16.2	28.9	29.5	22.3	37.1	31.7	16.1	20.9	8.6
≤ 15.5	16.4	4.2	3.4	6.9	3.4	27.9	24.2	25.9	19.4	18.6	31.9	32.6	24.6	40.3	34.7	18.1	23.2	9.4
≤ 18.5	18.2	4.6	3.7	7.5	3.6	31.4	27.1	28.8	21.7	21.3	35.1	35.7	26.9	43.5	37.7	20.2	25.1	10.3
≤ 21.5	19.7	5.0	3.9	8.1	3.8	34.6	29.5	31.5	23.7	23.8	38.0	38.5	29.1	46.3	40.3	22.2	27.0	11.1
≤ 25.0	21.4	5.6	4.2	8.7	3.9	38.0	32.1	34.5	25.0	26.6	41.0	41.5	31.3	49.1	43.2	24.4	30.4	12.0
≤ 30.0	23.5	6.1	4.5	9.6	4.2	42.5	35.3	38.4	28.0	30.2	44.8	45.4	34.2	52.7	46.8	27.5	33.5	13.4
≤ 37.5	26.3	7.1	5.0	11.1	4.6	48.3	39.5	43.8	33.1	35.1	49.8	50.5	38.2	57.4	51.5	31.7	37.0	15.4
≤ 45.0	28.9	8.2	5.6	12.7	5.3	53.1	43.2	48.5	36.9	39.5	53.9	54.9	41.7	61.2	55.6	35.8	42.2	17.6
≤ 52.5	31.2	9.2	6.2	14.6	6.1	57.2	46.5	52.7	40.4	43.5	57.5	58.7	44.9	64.5	59.2	39.7	45.7	19.7
≤ 62.5	34.1	10.7	7.0	17.2	7.4	61.7	50.4	57.5	44.7	48.3	61.5	63.1	48.7	68.2	63.1	44.4	50.1	22.4
≤ 75.0	37.7	12.5	8.2	20.6	9.2	66.1	54.6	62.5	49.5	53.5	65.6	67.6	52.7	71.8	67.0	49.7	54.8	25.4
≤ 90.0	42.0	14.7	9.9	24.7	11.6	70.3	59.0	67.5	54.5	58.9	69.5	72.0	56.8	75.1	70.6	55.2	59.6	28.8
≤ 105	46.1	16.9	11.8	28.9	14.4	73.7	62.9	71.9	59.0	63.5	72.8	75.6	60.5	77.7	73.6	60.0	63.8	32.2
≤ 125	51.5	20.1	14.9	34.6	18.8	77.4	67.8	76.7	64.5	68.8	76.7	79.6	64.9	80.7	76.4	65.6	68.6	36.6
≤ 150	57.8	25.0	19.8	41.6	25.3	81.6	73.5	81.5	70.7	74.6	80.9	83.6	69.9	83.8	79.4	71.7	73.9	42.3
≤ 180	64.9	32.4	27.6	50.0	34.5	85.9	79.9	86.3	77.6	80.6	85.4	87.7	75.2	87.1	82.4	78.1	79.5	49.4
≤ 215	72.6	42.9	38.8	59.7	46.4	90.2	86.5	90.7	84.7	86.4	89.8	91.4	80.7	90.7	85.4	84.6	85.4	57.9
≤ 255	80.4	56.5	52.7	70.2	60.3	93.8	92.4	94.4	91.3	91.7	93.9	94.5	86.0	94.1	88.6	90.5	91.1	67.6
≤ 305	88.7	73.8	69.8	81.6	76.1	96.9	97.2	97.3	96.7	96.1	97.2	97.0	91.1	97.4	92.1	95.7	96.2	78.9
≤ 365	95.6	90.4	86.3	91.5	90.2	98.5	99.7	99.1	99.	99.2	99.6	98.6	95.5	99.2	95.7	99.5	99.4	89.6
≤ 435	98.9	98.6	97.1	97.5	97.9	99.4	100.0	99.7	100.0	99.9	100.0	99.4	98.0	99.9	98.2	100.0	100.0	96.5
≤ 515	99.9	99.9	99.8	99.8	99.9	99.9		99.9		100.0		99.9	99.6	100.0	99.5			99.6
≤ 615	100.0	100.0	100.0	100.0	100.0	100.0		100.0				100.0	100.0		99.9			100.0
															100.0			

Particle size parameters	NBT1	NBT2	NBT3	NBT4	NBT5	NBT6	NBT7	NBT8	NBT9	NBT10	NBT11	NBT12	NBT13	NBT14	NBT15	NBT16	NBT17	NBT18
d_{10}	0.007	0.054	0.09	0.031	0.08	0.004	0.005	0.004	0.006	0.072	0.0028	0.0028	0.0041	0.0011	0.0024	0.0068	0.0043	0.017
d_{25}	0.033	0.14	0.17	0.09	0.14	0.013	0.017	0.013	0.022	0.022	0.01	0.0098	0.016	0.0065	0.0084	0.025	0.018	0.073
d_{50}	0.12	0.22	0.23	0.18	0.21	0.04	0.063	0.048	0.078	0.068	0.038	0.038	0.067	0.025	0.033	0.073	0.068	0.18
d_{60}	0.15	0.26	0.27	0.21	0.24	0.058	0.092	0.067	0.11	0.093	0.058	0.054	0.11	0.042	0.053	0.11	0.09	0.22
d_{75}	0.22	0.31	0.32	0.28	0.30	0.11	0.16	0.11	0.17	0.15	0.11	0.11	0.18	0.09	0.11	0.16	0.16	0.28
d_{90}	0.31	0.34	0.38	0.34	0.34	0.21	0.23	0.21	0.23	0.23	0.21	0.20	0.29	0.21	0.28	0.23	0.23	0.34
mean	0.127	0.225	0.245	0.185	0.220	0.062	0.089	0.062	0.096	0.086	0.060	0.060	0.098	0.048	0.059	0.093	0.089	0.177
S_0	2.58	1.48	1.37	1.76	1.46	2.91	3.07	2.91	2.78	2.61	3.32	3.35	3.35	3.72	3.62	2.53	2.98	1.96
U	21.43	4.81	3.00	6.77	3.00	14.50	18.40	17.00	18.33	1.29	20.71	19.29	26.83	38.18	22.08	16.18	20.93	12.94
S_k	0.50	0.90	1.03	0.78	0.95	0.89	0.69	0.62	0.61	0.71	0.76	0.75	0.64	0.94	0.85	0.75	0.62	0.63
K_{qa}	0.31	0.30	0.26	0.31	0.31	0.24	0.32	0.24	0.33	0.41	0.24	0.25	0.29	0.20	0.18	0.30	0.31	0.32

Density	NBT1	NBT2	NBT3	NBT4	NBT5	NBT6	NBT7	NBT8	NBT9	NBT10	NBT11	NBT12	NBT13	NBT14	NBT15	NBT16	NBT17	NBT18
(1)	106.66	100.57	97.09	103.65	97.09	109.12	101.81	141.82	134.50	97.68	128.65	132.36	133.13	120.91	108.70	131.97	130.53	113.89
(2)	1.33	1.26	1.21	1.30	1.22	1.36	1.27	1.77	1.68	1.22	1.61	1.65	1.66	1.51	1.36	1.65	1.63	1.42
(3)	2.22	2.10	2.02	2.16	2.03	2.27	2.12	2.95	2.80	2.04	2.68	2.76	2.77	2.52	2.26	2.75	2.72	2.37
(4)	3.19	2.20	2.03	2.50	2.39	2.20	2.14	2.07	5.77	2.62	2.16	3.27	2.39	2.28	2.18	4.20	4.18	4.43

Fraction A is characterized by median (d_{50}) values of 25 to 48 µm and corresponding mean values (($d_{25} + d_{75}$)/2) of 48 to 62 µm, reflecting material of largely coarse-silt size. The graphical coefficient of uniformity U ($U = d_{60}/d_{10}$) is between 14.50 and 38.18, indicating a non-uniform to very non-uniform particle size spectrum. A wide range of particle sizes, pointing to very poorly sorted material, is also reflected by sorting values (S_0; with $S_0 = \sqrt{(d_{75}/d_{25})}$) of 2.91 to 3.72. Skewness S_k ($S_k = (d_{75} + d_{25})/(d_{50})^2$) is consistently strongly positive, with all values ≥ 0.62. Kurtosis K_{qa} ($K_{qa} = (d_{75} - d_{25})/(2(d_{90} - d_{10}))$ is consistently ≤ 0.25 and thus very platykurtic. In contrast to Fraction A, Fraction B comprises material with d_{50} values of 63 to 180 µm and mean values of 86 to 185 µm, reflecting material of mainly fine-sand size. Like Fraction A, the fine-sand tailings material is largely very poorly sorted (S_0: 1.76–3.35), but U (U: 1.29–26.83) varies considerably between rarely uniform (one value), non-uniform (two values), and very non-uniform (six values). S_k is strongly positive (S_k: 0.50–0.78) and kurtosis (K_{aq}: 0.30–0.41) consistently very platykurtic. The medium-sand size material of Fraction C is characterized by d_{50} values of 210 to 230 µm and corresponding mean values of 220 to 240 µm. Although sorting is only poor, expressed by S_0 values of 1.37 to 1.49, the material has a uniform particle spectrum reflected by U values of ≤ 4.81. Like Fractions A and B, Fraction C has a strongly positive S_k (S_k: 0.90–1.03) and K_{aq} (K_{aq}: 0.26–0.31) is platykurtic.

The tailings material has a relatively uniform gross density, varying between 2.02 and 2.95 g/cm³ when using the powder density as base (data are provided in Table II). In contrast, the calculated density, based on geochemical and mineralogical data,

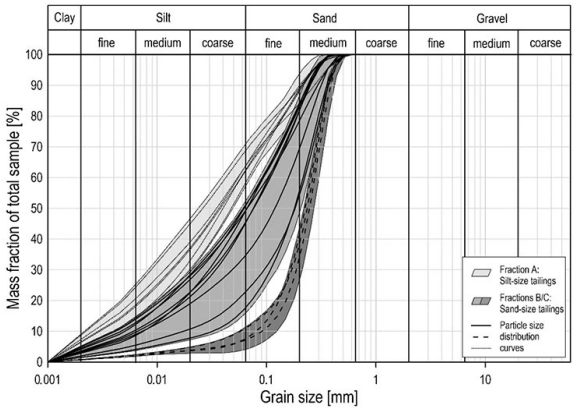

Figure 4—Particle size distribution curves of Namib Pb–Zn tailings based on laser diffraction data. The tailings material can be divided into three fractions based on median/mean values of 25–48 µm/48–62 µm (Fraction A), 63–180 µm/86–185 µm (Fraction B), and 210–230 µm/220–240 µm (Fraction C), reflecting material of largely coarse-silt, fine-sand, and medium-sand size, respectively. However, all fractions are, at most, poorly sorted

varies considerably between 2.90 and 5.77 g/cm^3, where most tailings samples have a calculated density in the range of 2.03 to 3.27 g/cm^3 and only four samples have a density > 4 g/cm^3. However, the mean density obtained by both semi-quantitative approaches is in a similar range of 2.4 to 2.9 g/cm^3, although a higher gross density does not necessarily correspond to a higher calculated density.

Tailings mineralogy

Namib Pb–Zn tailings are fine-grained, with most material in the coarse silt to fine sand fraction, which precludes the direct macroscopic and microscopic identification of the mineralogical phases present. Relict galena, sphalerite, pyrite, pyrrhotite, magnetite, hematite, calcite, and siderite were identified using XRD (Figure 4; Table III). However, differentiation of Ca–Mg–Fe(–Mn)-bearing carbonate phases is difficult by XRD, so the presence of other carbonates, including dolomite–ankerite solid solutions, is very likely. Moreover, XRD indicates the presence of quartz, graphite, apatite, the micas biotite, phlogopite, and muscovite, as well as plagioclase, and chlorite, which belong to the primary host mineral assemblage. In contrast, gypsum, lepidocrocite, and anglesite are interpreted to result from post-processing weathering under arid conditions. Some goethite is probably also of secondary origin; however, most goethite and jarosite originate from gossans mined at surface. The origins of rare anhydrite, chalcocite, and halite remain dubious. Halite likely results from evaporation of processing water and chalcocite is a common weathering product of primary copper minerals. Anhydrite might result from dehydration of gypsum. The presence of other minor and trace phases cannot be excluded, but identification is difficult at abundances of < 5 vol.% or the lack of a distinctive XRD pattern (e.g., anglesite, gypsum; Khan et al., 2020). Overall, the tailings mineralogy is similar to that of the primary ore, highlighting the fact that the former processing technologies, including flotation and the used flotation agents, did not modify the mineralogical assemblage.

Tailings geochemistry and bulk enrichment

The chemical composition ranges of the tailings samples are given in Figure 3A, showing major elements analysed by XRF, S by IR, and minor and trace elements by ICP–MS and AES. The older tailings are mainly composed of Fe (~ 16–31 mass%), Ca (~ 9–19 mass%), and minor Si (~ 3–7 mass%), Mn (~ 1–3 mass%), and Al (~ 1–2 mass%). K, Mg, Na, P, and Ti contents are insignificant, with average values < 0.6 mass%. Calculating all Ca as $CaCO_3$ and all Fe as $FeCO_3$ would translate into an average 35 mass% content of calcite and 41 mass% content of siderite in tailings, explaining the extremely high LOI values of ~ 9 mass% to 20 mass%. The tailings are very rich in S, which ranges from ~ 6.5 to 14.6 mass%, attributed

Table III

X-ray diffraction results of Namib Pb–Zn tailings (samples starting with NBT-) and primary Namib Pb–Zn ore (samples starting with NAM-)

Sample	Galena	Pyrite	Pyrrhotite	Sphalerite	Hematite	Magnetite	Apatite	Biotite	Chlorite	Microcline	Muskovite	Phlogopite	Graphite	Quartz	Calcite	Ca-Mg-Fe(-Mn) carbonates	Goethit	Jarosite	Lepidokrokite	Anglesite	Anhydrite	Chalcocite	Gypsum	Halite
NBT-1		x				x					x			x	x		x						x	
NBT-2			x	x		x		x	x				x		x		x		x				x	
NBT-3			x	x				x	x					x	x				x	x			x	
NBT-4			x	x					x		x			x	x	x	x		x				x	
NBT-5				x		x		x	x					x	x	x	x		x				x	
NBT-6			x	x		x			x			x		x	x								x	
NBT-7	x		x	x						x		x		x	x				x				x	
NBT-8		x	x	x							x			x	x	x							x	
NBT-9	x		x	x				x						x	x					x			x	
NBT-10			x	x							x			x	x			x			x	x	x	x
NBT-11			x									x		x	x					x			x	
NBT-12			x	x				x					x		x	x				x			x	
NBT-13			x	x	x		x		x		x			x	x								x	
NBT-14			x	x				x						x	x	x								
NBT-15			x	x					x		x			x	x	x								
NBT-16	x		x	x				x						x	x									
NBT-17	x	x	x	x			x	x			x		x		x									
NBT-18	x	x	x	x		x					x			x	x		x							
NAM-1	x	x		x								x			x									
NAM-2	x	x		x								x			x									

to the presence of sulfide mineral phases and minor sulfates. The primary Pb–Zn ore signature is reflected by high Pb and Zn values of ~ 0.2 to 5.7 mass% (av. 1.2 mass%) and ~ 0.9 to 9.6 mass% (av. ~3.2 mass%), respectively, classifying them as major components in these tailings. Tailings show high contents (av. values > 100 µg/g) of Cu, Sr, As, and Cd. In addition, Ba, Rb, W, Ce, Sn, Ag, La, Sb, In, Nd, Ni, Co, Li, Cr, and V values are > 10 µg/g. Average Cs and Bi values are slightly below 10 µg/g. This indicates that minor to very low concentrations of the critical elements (As,) Bi, Cs, In, Sb, Sn, and W, which are essential for modern economy but are very vulnerable to supply disruptions in the mining chain according to the classification of the USGS (2018), and noteworthy Zn and Pb proportions are still present in these tailings. (Arsenic was formerly ranked amongst the critical elements, which was later modified, and is therefore shown in brackets).

Compared with average crustal abundance (data from Rudnick and Gao, 2003), Namib Pb–Zn tailings are significantly enriched in Cd (~ 1660× on av.). Pb, (~ 1050×), Zn (~ 445×), Ag (~ 400×), In (~ 280×), and S (~ 250×). Sb (~ 75×), As (~ 72×), Bi (~ 50×), and W (~ 50×) show also a distinct enrichment. However, W values have to be regarded as semi-quantitative, because a WC mill was used for pulp preparation, but accessory scheelite is detected in primary Namib Pb–Zn ore. A moderate to slight enrichment is also observed for Cu (18×), Sn (15×), and Cs (5×). All other elements show no notable enrichment or have averages close to crustal abundance or even below. Amongst the most enriched elements in Namib Pb–Zn tailings is the critical element In (80–770×). In addition, the critical elements Sb (~ 20–220×), As (~ 35–240×), W (~ 30–70×), and Bi (~15–250×) are distinctly enriched, and Cs (2–14×) shows a minor enrichment (Figure 3B).

Discussion

Geochemical relations

Principally, the general geochemical compositions of primary Namib Pb–Zn ore and related tailings material are similar for several elements, however, the relative proportions of some elements deviate due to the extraction of sphalerite and galena, and associated elements. Consequently, primary ore has at least 10× higher Zn, 7× higher Cd concentration, and about 6× higher In concentration than tailings material, based on our data. In contrast, the chalcophile elements As, Bi, and Cu have distinctly to slightly higher concentrations in tailings material than in primary ore samples (~ 125–5×). Likewise, slightly higher concentrations in tailings material are shown by Cs, Ta, W, and Li (14–5×). However, a slight bias due to contamination during milling cannot be excluded

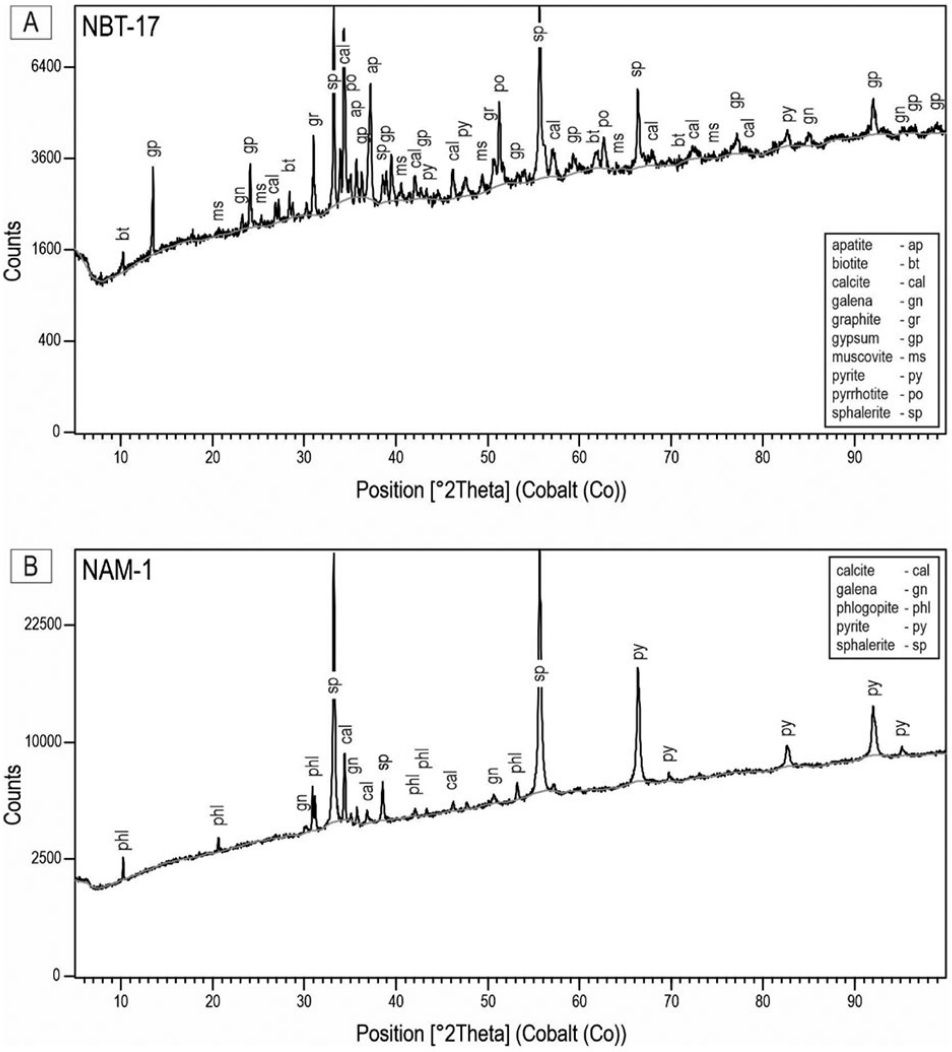

Figure 5—Selected X-ray diffraction results of Namib Pb–Zn tailings and primary Namib Pb–Zn ore. A: Indexed XRD pattern of tailings sample NBT-11. B: Indexed XRD pattern of primary ore sample NAM-1

for W and the primary ore database is small. All other elements occur in similar concentration ranges in primary ore as well as in tailings.

Reprocessing potential of Namib tailings

The tailings composition directly reflects the primary ore mineralogy, although mineral abundances have been modified due to the extraction of the mineral(s) of interest (i.e., sphalerite, galena) in a quantitative sense. Post-processing weathering resulted only in the formation of rare sulfates and probably some Fe-hydroxides. Namib Pb–Zn tailings have not been subject to any pyrometallurgical modification because only a simple classical enrichment/concentration of ore material was done. The focus during the first years was on the production of a galena concentrate; production later included a sphalerite concentrate and by-product Ag of undescribed origin. One major attempt of extracting sphalerite from the old tailings dump in the mid-1990s led to the construction of the younger tailings dump (Hahn et al., 2004). However, processing technology was less advanced in the 1990s than today and extraction of noteworthy quantities of sphalerite failed due to problems with pyrrhotite suppression during flotation (Snowden, 2014).

Today, processing of Zn-Pb(-Cu) ores is still the most complex of all ore types because processing characteristics have to be adjusted to individual ore characteristics (Bulatovic, 2007) and Pb production can have hazardous impacts on the environment and human health (Nayak et al., 2021). However, during the last 20 years, no new large Pb–Zn deposits have been exploited (Mudd et al., 2017), so recovery from existing resources becomes important because both metals are wanted on international markets. In particular, processing of pyrrhotite-bearing Zn–Pb(–Cu) ore is challenging because Fe-rich sphalerite behaves very similarly to pyrrhotite (e.g., Tang and Chen, 2022), so a sequential or differential (froth) flotation approach has to be chosen. During sequential flotation, (Cu–)Pb minerals are first floated and recovered and then Zn minerals are activated (e.g., Lang et al., 2018), with pyrrhotite going into the rejects. If Pb minerals have to be separated from Cu minerals, then this is done on upgraded bulk concentrate (Bulatovic, 2007). Another processing approach is by bulk (Cu–)Pb–Zn mineral flotation followed by (Cu–)Pb–Zn mineral separation (e.g., Basilio et al., 1996; Luo et al., 2016), with pyrrhotite going into the rejects. The sequential approach usually performs better when precious metals, like Ag, should be recovered (Bulatovic, 2007). In contrast, bulk (Cu–)Pb–Zn mineral flotation is, in general, more economic (Bulatovic, 2007) and more suitable for low-grade sulfide ores with complex mineral intergrowths (e.g., Lang et al., 2018). Different reagent schemes have been successfully tested in recent years, including bisulfide, starch/lime, and soda ash/SO_2 or lime/SO_2 methods for the sequential approach. A combination of different depressants, including NaCN, ammonium sulfate, and $ZnSO_4$ was tested successfully for bulk flotation of different Pb–Zn(–Cu) ores with Fe-rich sphalerite and high pyrrhotite contents (Bulatovic, 2007; Bulatovic and Wyslouzil, 1995, 1999; Tang and Chen, 2022; Wang et al., 2019). However, the collectors most currently used are xanthates and dithiophosphates (e.g., Kohad, 1998; Li and Zhang, 2012; Tang and Chen, 2022; Yuan et al., 2012) with sodium polyacrylate and/or sodium hexametaphosphate as dispersants for sphalerite flotation (e.g., Silvestre et al., 2009) and pine oil as frother (Nayak et al., 2021) because cyanides and other formerly used chemicals are effective, but toxic (e.g., Lang et al., 2018; Nayak et al., 2021). Flotation is performed at high alkalinity (pH 10.5–12) to prevent activation of pyrrhotite (Tang and Chen, 2022; Wills and Napier-Munn, 2005) and a pre-aeration prior to the addition of a collector was successfully performed to lower the floatability of pyrrhotite (e.g., Becker et al., 2010; Tang and Chen, 2022). Moreover, flotation columns are nowadays recommended because recovery of finely disseminated mineral particles is more effective on columns than via the traditional flotation cells (Kursun and Ulusoy, 2012; Lang et al., 2018; Mittal et al., 2000). In addition, there are promising approaches using high-gradient magnetic separators to pre-concentrate Fe-rich sphalerite and to separate Fe-rich sphalerite and pyrrhotite (e.g., Jeong and Kim, 2018) because the magnetic susceptibility of sphalerite increases with increasing Fe content (e.g., Keys et al., 1968; Pearce et al., 2006).

Flotation of highly variable ore with pyrrhotite, quartz, dolomite, and siderite was successfully performed, for example, at the Renison Bell tin mine, Tasmania, with desliming conducted at 6 µm, and old tailings of the South African Union and Rooiberg mines, South Africa, were also successfully floated (Bulatovic, 2010). During recent years, mining and recovery of the remaining low-grade Rosh Pinah, Namibia, Zn–Pb ore (cut-off Zn 3.0%, cut-off Pb 1.95%) with trace to minor amounts of pyrrhotite and chalcopyrite (Alchin and Moore, 2005; Fourie et al., 2007) was successfully tested. A selective approach was chosen (Sehlotho et al., 2018) to produce Zn and Pb mineral concentrates. In general, Zn mineral concentrate from Rosh Pinah was exported to the South African Zincor smelter in Springs, while the Pb mineral concentrate was traded on the international markets (Fourie et al., 2007). A similar approach also seems feasible for Namib Pb–Zn tailings.

The older Namib Pb–Zn tailings dump comprises ca. 2.75 Mm^3 of re-processible material with average Zn and Pb contents of 3.20 mass% and 1.15 mass%, respectively, based on our preliminary data, so Zn and Pb will be the principal targets during reprocessing. The tailings contain minor In (av. 14 µg/g in bulk sample) and Sb (av. 15 µg/g in bulk sample), two critical elements, which are of interest for modern 'green' industry applications. In addition, there is some Ag (av. 22 µg/g in tailings) in galena (Lohmeier et al., 2024), which is an economically attractive by-product, and Cd (av. 133 µg/g in bulk sample) in sphalerite (Lohmeier et al., 2024). Ag and Cd will be directly extracted as part of sphalerite and galena during production of saleable (combined) Pb and Zn concentrates. Smelting and production of pure metals on site at Swakopmund or at the Tsumeb smelter, the only smelter in Namibia—focussed on the production of Pb and Cu from sulfidic ore (Lohmeier et al., 2021a and references therein)—is probably not feasible. However, there are smelters abroad capable of smelting carbonate-hosted base metal concentrates to obtain Pb, Zn, and by-products, such as Ag, Sb, and In (see Alfantazi and Moskalyk, 2003); Zn concentrates of variable composition were previously processed at the South African Zincor smelter (Van Niekerk and Begley, 1991). Extraction of the contained critical commodities (As,) Bi, and Cs is not feasible as concentrations are very low. Production of by-product Ag and Cd might be feasible. Considering a remaining combined measured and indicated tailings tonnage of about 610 000 t (NLZM, 2023), this would translate into a resource containing about 19 530 t Zn, 7 030 t Pb, 14 t Ag, 9 t Sb, and 9 t In, plus 300 t Cu and 80 t Cd. However, using the determined average gross density of about 2.42 g/cm^3 (2.90 g/cm^3; results obtained by the calculated density are shown in brackets) and the tailings resource outlined by Hahn et al. (2004) of 2.75 Mm^3, this would translate into a tonnage of ~ 6.65 Mt (~ 7.97 Mt) containing about 213 100 t Zn (255 350 t

Zn), 76 680 t Pb (91 900 t Pb), 3260 t Cu (3900 t Cu), 885 t Cd (1060 t Cd), 150 t Ag (180 t Ag), 98 t Sb (120 t Sb), and 95 t In (115 t In). This distinct discrepancy between the two resource estimates can be explained by lacking company data for the inferred tailings resource. Our data distinctly deviate from that provided by Hahn et al. (2004), with average element values of 2.54% Zn, 0.21% Pb, and 7.0 g/t Ag for the old tailings dumps, and from data provided from NLZM (2023), with average element values of 0.3% Pb, 2.2% Zn, and 7.5 g/t Ag for the combined measured and indicated tailings resource. These differences are due to the fact that we took mostly surface samples, which are representative of the surficial part of the old tailings dump, but are not necessarily representative for the bulk of the tailings pile, whereas data by NLZM (2023) and Hahn et al. (2004) are largely based on drilling activities. Thus, some bias might be induced by wind erosion removing less dense particles and leaving heavier ones behind. Nevertheless, it becomes clear that the Namib Pb–Zn tailings dump represents a noteworthy metal resource. Future resource and reserve estimates should establish tailings heterogeneities and zonations.

This study demonstrates that tailings characterization solely relying on XRD and bulk geochemical data of tailings can be misleading. For example, the XRD data of Namib Pb–Zn tailings do not indicate the presence of rare to accessory marcasite, cassiterite, and scheelite, which have been detected in primary ore. Moreover, the bulk geochemical data do not reveal the siting of trace elements (Lohmeier et al., 2024). Therefore, whenever possible, assessment of fine-grained tailings, like slurries and impoundment cell material, should not be performed solely on tailings, but should be combined with (detailed) mineralogical and geochemical investigations of primary ore and host rock(s). It is quite likely that marcasite, cassiterite, and scheelite were not detected by XRD because concentrations are low and all three minerals do not have striking XRD patterns (see Khan et al., 2020). However, if larger quantities of pyrite or marcasite were erroneously overlooked, a potential risk for AMD would stay undetected.

On the one hand, the old Namib Pb–Zn tailings dump contains a certain resource that is of economic interest (Ag, Cd, Pb, Zn; e.g., Mudd et al., 2017; Werner et al., 2017); on the other hand, the tailings dump is a contamination source of environmentally significant As, Pb, and Cd, which may become hazardous to humans and the environment (Mudd et al., 2017). North River Resources cleaned the mine site in the late 2000s, however, the principal source of pollution remains as long as it is not safely sealed from wind erosion (e.g., Blight, 2007; Salom and Kivinen, 2019). The effects of climate change on metal mobility from mine waste repositories are difficult to estimate (Northey et al., 2017). Currently, tailings dispersal only affects the immediate surroundings, but strong winds, temporal rainfalls, and potential seepage may mobilize environmentally significant As, Pb, and Cd into surface soils, sediments, as well as ground and surface waters. Reprocessing of the Namib tailings would have obvious environmental as well as economic benefits. In fact, the southern African mineral processing industry has demonstrated that it is capable to recover additional metals from old tailings dumps (e.g., Craven, 2001; Guest et al., 1988; Jones et al., 2002; Svoboda et al., 1988; Watson and Beharrell, 2006).

Conclusion

Clay- to sand-sized Namib Pb–Zn tailings were produced during mineral processing in the 1960–1990s of sphalerite–galena–pyrite ore, which also contained minor pyrrhotite, rare marcasite, cassiterite, and arsenopyrite, as well as accessory scheelite set into a carbonate-rich host rock. In addition to Pb and Zn, the older tailings dump contains trace concentrations of the critical elements In and Sb. Ag and Cd could be extracted and concentrated together with Pb and Zn. Any future processing of Pb–Zn(–Cu) tailings would be challenging, and might result in a combined Pb–Zn mineral concentrate or even two separate Pb and Zn mineral concentrates with valuable by-products. It is not realistic that the old tailings dump will soon be the sole target on the Namib Pb–Zn mining site, but it is definitely worth considering reprocessing when mining and extraction of primary Pb–Zn ore continue. Presently, the historic tailings dumps are not covered and are therefore considered as a point source of ongoing metal contamination. Consequently, any reprocessing of tailings, with subsequent disposal of wastes in an appropriately designed mine waste repository, would also eliminate a major metal pollution source. Pb–Zn-containing base metal tailings dumps have to be considered as secondary raw material sources following the principle of circular economy.

Acknowledgements

This work was supported by the German Federal Ministry of Education and Research (BMBF) and is part of the sub-Saharan based LoCoSu project; grant number 01DG16011. We thank S. Garoeb and M. Punzel from Namib Pb–Zn for free access to the sampling site in 2018 and for an exciting above-ground mine visit in 2019. U. Hemmerling is thanked for preparation of polished (thin) sections (Clausthal University of Technology (TUC), Department of Mineral Resources (IMMR)) and we are grateful to L. Weitkämpfer, D. Gürsel, and P. Ihl (RWTH Aachen University, Department of Processing) for providing free access to powder preparation equipment and their never-ending patience. Thanks to M. Gamenik (Institute of Mineral and Waste Processing, Recycling and Circular Economy Systems, TUC) for assistance with laser diffractometry.

Authors contribution

Conceptualization: BGL, SL; sampling: DG, SL; methodology: DG, SL; validation: SL; formal analysis: SL; data curation: SL; writing - original draft preparation: SL; writing - review and editing: DG, BGL; funding acquisition: BGL

References

Alchin, D.J., Moore, J.M. 2005. A review of the Pan-African, Neoproterozoic Rosh Pinah Zn-Pb deposit, southwestern Namibia. *South African Journal of Geology*, vol. 108, pp. 71–86. https://doi.org/10.2113/108.1.71

Alfantazi, A.M., Moskalyk, R.R. 2003. Processing of indium: A review. *Minerals Engineering*, vol. 16, pp. 687–694. https://doi.org/10.1016/S0892-6875(03)00168-7

Badenhorst, F.P. 1987. Lithostratigraphy of the Damara sequence in the Omaruru area of the Northern Central Zone of the Damara Orogen and a proposed correlation across the Omaruru Lineament. *Communications of the Geological Survey of Namibia*, vol. 3, pp. 3–9.

Basilio, C.I., Kartio, I.J., Yoon, R.-H. 1996. Lead activation of sphalerite during galena flotation. *Mineral Engineering*, vol. 9, pp. 869–879. https://doi.org/10.1016/0892-6875(96)00078-7

Basson, I.J., McCall, M.-J., Andrew, J., Dawerti, E. 2018. Structural controls on mineralisation at the Namib Lead and Zinc Mine, Damara Belt, Namibia. *Ore Geology Reviews*, vol. 95, pp. 931–944. https://doi.org/10.1016/j.oregeorev.2018.03.028

Becker, M., de Villiers, J., Bradshaw, D. 2010. The flotation of magnetic and non-magnetic pyrrhotite from selected nickel ore deposits. *Minerals Engineering*, vol. 23, pp. 1045–1052. https://doi.org/10.1016/j.mineng.2010.07.002

Beuselinck, L., Govers, G., Poesen, J., Degraer, G., Froyen, L. 1998. Grain-size analysis by laser diffractometry: comparison with the sieve-pipette method. *Catena*, vol. 32, pp. 193–208. https://doi.org/10.1016/S0341-8162(98)00051-4

Blight, G.E. 2007. Wind erosion of tailings dams and mitigation of the dust nuisance. *Journal of the South African Institute of Mining and Metallurgy*, vol. 107, pp. 99–107.

Bulatovic, S.M. 2007. Flotation of sulfide ores. *Handbook of Flotation Reagents: Chemistry, Theory and Practice*. Bulatovic, S.M. (ed.). Elsevier, Amsterdam. pp. 367–400. https://doi.org/10.1016/C2009-0-17332-4

Bulatovic, S.M. 2010. Flotation of tin minerals. *Handbook of Flotation Reagents: Chemistry, Theory and Practice*. Bulatovic, S.M. (ed.). Elsevier, Amsterdam. pp. 87–109. https://doi.org/10.1016/C2009-0-17332-4

Bulatovic, S.M., Wyslouzil, D.M. 1995. Selection and evaluation of different depressants systems for flotation of complex sulphide ores. *Minerals Engineering*, vol. 8, pp. 63–76. https://doi.org/10.1016/0892-6875(94)00103-J

Bulatovic, S.M., Wyslouzil, D.M. 1999. Development and application of new technology for the treatment of complex massive sulphide ores – case study – Faro lead/zinc concentrator – Yukon. *Minerals Engineering*, vol. 12, pp. 129–145. https://doi.org/10.1016/S0892-6875(98)00127-7

Colin Christian and Associates CC (CCA). 2013. Proposed recommissioning of Lead and Zinc Mine on EPL 2902. Volume 1: Environmental impact assessment and environmental management plan including closure and rehabilitation.

Craven, P.M. 2001. International Patent Number WO 01/16385 A1. Base metal recovery from a tailings dump by bacterial oxidation.

Dachroth, W. 2017. *Handbuch der Baugeologie und Geotechnik*. Springer, Berlin. https://doi.org/10.1007/978-3-662-46886-9

DIN 18300. 2019. VOB Vergabe- und Vertragsordnung für Bauleistungen. Beuth.

Dold, B. 2010. Basic concepts in environmental geochemistry of sulfidic mine-waste management. *Waste Management*. Kumar, E.S. (ed.). InTech, pp. 173–198.

European Commission. 2010. Critical raw materials for the EU. Report of the ad-hoc working group on defining critical raw materials. European Commission, Brussels.

European Commission. 2017. Study on the review of the list of critical raw materials – criticality assessments. European Commission, Brussels.

Festin, E.S., Tigabu, M., Chileshe, M.N., Syampungani, S., Odén, P.C. 2019. Progresses in restoration of post-mining landscape in Africa. *Journal of Forestry Research*, vol. 30, pp. 381–396. https://doi.org/10.1007/s11676-018-0621-x

Fourie, H., Van Rooyen, P.H., Rupprecht, S., Kund, T., Vegter, N.M. 2007. Exploitation of a massive low grade zinc-lead resource at Rosh Pinah zinc corporation, Namibia. *Proceedings of the Fourth Southern African Conference on Base Metals*, South African Institute of Mining and Metallurgy, Johannesburg. pp. 109–118.

Frimmel, H.E., Miller, R.McG. 2009. Mineral deposits. *Developments in Precambrian Geology*, vol. 16, pp. 227–229. https://doi.org/10.1016/S0166-2635(09)01616-8

Guest, R.N., Svoboda, J., Venter, W.J.C. 1988. The use of gravity and magnetic separation to recover copper and lead from Tsumeb flotation tailings. *Journal of the South African Institute of Mining and Metallurgy*, vol. 88, pp. 21–26.

Hahn, L., Solesbury, F., Mwiya, S. 2004. Report: Assessment of potential environmental impacts and rehabilitation of abandoned mine sites in Namibia. *Communications of the Geological Survey of Namibia*, vol. 13, pp. 85–91.

Harrison, S., Broadhurst, J., Van Hille, R., Oyekola, O., Bryan, C., Hesketh, A., Opitz, A., 2010. A systematic approach to sulphidic waste rock and tailings management to minimise acid rock drainage formation. Report to the Water Research Commission. WRC Report No. 1831/1/10.

Jahanshahi, S., Bruckard, W., Somerville, M. 2007. Towards zero waste and sustainable resource processing. *International Conference on Processing and Disposal of Mineral Industry Waste 2007* (PDMIW'07), Falmouth.

Jeong, S., Kim K. 2018. Pre-concentration of iron-rich sphalerite by magnetic separation. *Minerals*, vol. 8, no. 272. https://doi.org/10.3390/min8070272

Jones, R.T., Denton, G.M., Reynolds, Q.G., Parker, J.A.L., Van Tonder, G.J.J. 2002. Recovery of cobalt from slag in a DC arc furnace at Chambishi, Zambia. *Journal of the South African Institute of Mining and Metallurgy*, vol. 102, pp. 5–9.

Keys, J.D., Horwood, J.L., Baleshta, T.M., Cabri, L.J., Harris, D.C. 1968. Iron-iron interaction in iron-containing zinc sulphide. *Canadian Mineralogist*, vol. 9, pp. 453–467.

Khan, H., Yerramilli, A.S., D'Oliveira, A., Alford, T.L., Boffito, D.C., Patience, G.S. 2020. Experimental methods in chemical engineering: X-ray diffraction spectroscopy – XRD. *Canadian Journal of Chemical Engineering*, vol. 98, pp. 1255–1266. https://doi.org/10.1002/cjce.23747

Kohad, V.P. 1998. Flotation of sulphide ores – HZL experience. *Froth Flotation: Recent Trends*. Indian Institute of Minerals Engineering, Jamshedpur, pp. 18–41.

Konert, M., Vandenberghe, J. 1997. Comparison of laser grain size analysis with pipette and sieve analysis: a solution for the underestimation of the clay fraction. *Sedimentology*, vol. 44, pp. 523–535. https://doi.org/10.1046/j.1365-3091.1997.d01-38.x

Kursun, H., Ulusoy, U. 2012. Zinc recovery from lead-zinc-copper complex ores by using column flotation. *Mineral Processing and Extractive Metallurgy Review*, vol. 33, pp. 327–338. https://doi.org/10.1080/08827508.2011.601479

Lang, J.-T., Liu, S.-Q., Dong, X., Pei, Y. 2018. Current situation on flotation of Cu-Pb–Zn sulfide ore. *Advances in Engineering Research*, vol. 120, pp. 1972–1976. https://doi.org/10.2991/ifeesm-17.2018.355

Laurence, D. 2011. Establishing a sustainable mining operation: an overview. *Journal of Cleaner Production*, vol. 19, pp. 278–284. https://doi.org/10.1016/j.jclepro.2010.08.019

Lèbre, E., Corder, G.D., Golev, A. 2016. Sustainable practices in the management of mining waste: a focus on the mineral resource. *Minerals Engineering*, vol. 107, pp. 34–42. https://doi.org/10.1016/j.mineng.2016.12.004

Lehtonen, M.I., Manninen, T.E.T., Schreiber, U.M. 1996. Report: Lithostratigraphy of the area between the Swakop, Khan and lower Omaruru Rivers, Namib desert. *Communications of the Geological Survey of Namibia*, vol. 11, pp. 71–82.

Lei, C., Yan, B., Chen, T., Quan, S.-X., Xiao, X.-M. 2015. Comprehensive utilization of lead-zinc tailings, part 1: Pollution characteristics and resource recovery of sulfur. *Journal of Environmental Chemical Engineering*, vol. 3, pp. 862–869. https://doi.org/10.1016/j.jece.2015.03.015

Li, M., Zhang, Q. 2012. Experimental study on flotation process conditions of lead-zinc ore. *Advanced Materials Research*, vol. 454, pp. 183–188. https://doi.org/10.4028/www.scientific.net/AMR.454.183

Liakopoulos, A., Lemière, B., Michael, K., Crouzet, C., Laperche, V., Romaidis, I. Drougas, I., Lassin, A. 2010. Environmental impacts of unmanaged solid waste at a former base metal mining and ore processing site (Kirki, Greece). *Waste Management and Research*, vol. 28, pp. 996–1009. https://doi.org/10.1177/0734242X10375746

Lohmeier, S., Lottermoser, B.G., Schirmer, T., Gallhofer, D. 2021. Copper slag as a potential source of critical elements – a case study from Tsumeb, Namibia. *Journal of the Southern African Institute of Mining and Metallurgy*, vol. 121, pp. 129–142. http://dx.doi.org/10.17159/2411-9717/1383/2021

Lohmeier, S., Gallhofer, D., Lottermoser, B.G. 2024. Field-portable X-ray fluorescence analyzer for chemical characterization of carbonate-bearing base metal tailings: case study from Namib Pb-Zn Mine, Namibia. *Journal of the South African Institute of Mining and Metallurgy*, vol. 124, no. 8, pp. 421–436.

Luo, X., Feng, B., Wong, C., Miao, J., Ma, B., Zhou, H. 2016. The critical importance of pulp concentration on the flotation of galena from a low grade lead-zinc ore. *Journal of Materials Research and Technology*, vol. 5, pp. 131–135. https://doi.org/10.1016/j.jmrt.2015.10.002

Lupankwa, K., Love, D., Mapani, B., Mseka, S. 2004. Impact of a base metal slimes dam on water systems, Madziwa Mine, Zimbabwe. *Physics and Chemistry of the Earth*, vol. 29, pp. 1145–1151. https://doi.org/10.1016/j.pce.2004.09.017

Miller, R.McG. 2008. Neoproterozoic and early Palaeozoic rocks of the Damara Orogen in Miller. *Geology of Namibia*. R. Miller McG. (ed.). Ministry of Mines and Energy, Geological Survey of Namibia, 13-1–13-433.

Miller, B.A., Schaetzl, R.J. 2011. Precision of soil particle size analysis using laser diffractometry. *Soil Science Society of America Journal*, vol. 76, pp. 1719–1727. https://doi.org/10.2136/sssaj2011.0303

Ministry of Mines and Energy, Geological Survey of Namibia (MME). 1996. The Geology of Area 2214 – Walvis Bay. Explanations of Sheet 2214.

Mittal, N.K., Sen, P.K., Chopra, S.J., Jaipuri, A.A., Gaur, R.K., Jakhu, M.R. 2000. Technical note – India's first column flotation installation in the zinc cleaning circuit at Rajpura Dariba Mine, India. *Minerals Engineering*, vol. 13, pp. 581–584. https://doi.org/10.1016/S0892-6875(00)00038-8

Moreno, L., Neretnieks, I. 2006. Long-term environmental impact of tailings deposits. *Hydrometallurgy*, vol. 83, pp. 176–183. https://doi.org/10.1016/j.hydromet.2006.03.052

Mudd, G.M., Jowitt, S.M., Werner, T.T. 2017. The world's lead-zinc mineral resources: scarcity, data, issues and opportunities. *Ore Geology Reviews*, vol. 80, pp. 1160–1190. https://doi.org/10.1016/j.oregeorev.2016.08.010

Nayak, A., Jena, M.S., Mandre, N.R. 2021. Beneficiation of lead-zinc ores – a review. *Mineral Processing and Extractive Metallurgy Review*, vol. 43, pp. 1–20. https://doi.org/10.1080/08827508.2021.1903459

Namib Lead and Zinc Mining (NLZM). 2023. http://www.namibleadzinc.com/operations.html [Assessed 7 March 2023].

Northey, S.A., Mudd, G.M., Werner, T.T., Jowitt, S.M., Haque, N., Yellishetty, M., Weng, Z. 2017. The exposure of global base metal resources to water criticality, scarcity and climate change. *Global Environmental Change*, vol. 44, pp. 109–124. https://doi.org/10.1016/j.gloenvcha.2017.04.004

Pearce, C.I., Pattrick, R.A.D., Vaughan, D.J. 2006. Electrical and magnetic properties of sulfides. *Reviews in Mineralogy and Geochemistry*, vol. 61, pp. 127–180. https://doi.org/10.2138/rmg.2006.61.3

Rudnick, R.L., Gao, S. 2003. Composition of the continental crust. *Treatise on Geochemistry*, vol. 3, pp. 1–64. https://doi.org/10.1016/B978-0-08-095975-7.00301-6

Salom, A.T., Kivinen, S. 2019. Closed and abandoned mines in Namibia: a critical review of environmental impacts and constraints to rehabilitation. *South African Geographical Journal*, vol. 102, pp. 1–17. https://doi.org/10.1080/03736245.2019.1698450

Sehlotho, N., Sindane, Z., Bryson, M., Lindvelt, L. 2018. Flowsheet development for selective Cu-Pb–Zn recovery at Rosh Pinah concentrator. *Minerals Engineering*, vol. 122, pp. 10–16. https://doi.org/10.1016/j.mineng.2018.03.001

Silvestre, M.O., Pereira, C.A., Galery, R., Peres, A.E.C. 2009. Dispersion effect on a lead-zinc sulphide ore flotation. *Minerals Engineering*, vol. 22, pp. 752–758. https://doi.org/10.1016/j.mineng.2008.12.009

SLR Environmental Consulting (SLR-EC). 2013. Namib Mine. Ground- and surface water specialist input for EIA report. Report no. 2031-GS-6.

Snowden. 2014. Namib lead zinc project. Project no. J2178. Mine development plan.

Souissi, R., Souissi, F., Chakroun, H.K., Bouchard, J.L. 2013. Mineralogical and geochemical characterization of mine tailings and Pb, Zn, and Cd mobility in a carbonate setting (Northern Tunisia). *Mine Water and the Environment*, vol. 32, pp. 16–27. https://doi.org/10.1007/s10230-012-0208-2

Svoboda, J., Guest, R.N., Venter, W.J.C. 1988. The recovery of copper and lead minerals from Tsumeb flotation tailings by magnetic separation. *Journal of the South African Institute of Mining and Metallurgy*, vol. 88, pp. 9–19. https://hdl.handle.net/10520/AJA0038223X_1865

Tang, X., Chen, Y. 2022. A review of flotation and selective separation of pyrrhotite: A perspective from crystal structures. *International Journal of Mining Science and Technology*, vol. 32, pp. 847–863. https://doi.org/10.1016/j.ijmst.2022.06.001

Tenova Mining and Minerals. 2014. North River Namib lead/zinc project. Feasibility Study, M8168-1300-001, Section: 2 Introduction and project background.

Unites States Geological Survey (USGS). 2018. Draft critical mineral list – summary of methodology and background information – U.S. Geological Survey technical input document in response to secretarial order no. 3359.

Van Niekerk, C.J., Begley, C.C. 1991. Zinc in South Africa. *Journal of the South African Journal of Mining and Metallurgy*, vol. 91, pp. 233–248.

Wang, H., Wen, S., Han, G., Feng, Q. 2019. Effect of copper ions on surface properties of $ZnSO_4$-depressed sphalerite and its response to flotation. *Separation and Purification Technology*, 228, no. 115756. https://doi.org/10.1016/j.seppur.2019.115756

Watson, J.H.P., Beharrell, P.A. 2006. Extracting values from mine dumps and tailings. *Minerals Engineering*, vol. 19, pp. 1580–1587. https://doi.org/10.1016/j.mineng.2006.08.014

West, J. 2020. Extractable global resources and the future availability of metal stocks: "known unknowns" for the foreseeable future. *Resources Policy*, 65, no. 101574. https://doi.org/10.1016/j.resourpol.2019.101574

Werner, T.T., Mudd, G.M., Jowitt, S.M. 2017. The world's by-product and critical metal resources part III: a global assessment of indium. *Ore Geology Reviews*, vol. 86, pp. 939–956. https://doi.org/10.1016/j.oregeorev.2017.01.015

Wills, B.A., Napier-Munn, T. 2005. *Will's Mineral Processing Technology*. Elsevier. https://doi.org/10.1016/C2010-0-65478-2w

ESGS ENVIRONMENTAL SOCIAL GOVERNANCE SUSTAINABILITY

SAIMM COMMITTEE
THE SOUTHERN AFRICAN INSTITUTE OF MINING AND METALLURGY

SAIMM
THE SOUTHERN AFRICAN INSTITUTE OF MINING AND METALLURGY

130 Years OF TECHNICAL EXCELLENCE

ESG IN THE MINERALS INDUSTRY CHALLENGES AND OPPORTUNITIES

DATE: 16-17 OCTOBER 2024
VENUE: GLENBURN LODGE AND SPA, MULDERSDRIFT

ECSA Validated CPD Activity, Credits = 0.1 points per hour attended.
**SACNASP Accreditation - One credit for every 10 hours attended.*

BACKGROUND

Environmental, Social, and Governance (ESG) considerations have become increasingly important in the business world, as it contributes to long-term sustainability and responsible corporate behaviour.

In the minerals industry, ESG considerations are particularly important due to the sector's significant environmental and social impacts. Mining operations involve land use, energy and water consumption, and waste generation, which have lasting effects on ecosystems. Additionally, the industry faces challenges related to labour practices, community engagement, and the impact on indigenous populations.

An ESG-driven strategy is not only a responsible approach to business but also a strategic imperative for long-term success. It can contribute to risk mitigation, enhances reputation, attracts capital, and fosters innovation, making it a competitive advantage in today's business landscape. In the mining industry, ESG considerations are crucial for addressing environmental and social challenges and ensuring the industry's sustainable development.

The role of the Southern African Institute of Mining and Metallurgy (SAIMM) in the promotion of ESG is based on the premise that sustainability, and the contribution of the mining and minerals industry to society, is dependent on the professional and ethical conduct of minerals industry professionals – our members.

On this basis, the purpose and focus of this conference is to influence professional behaviour, and foster industry dialogue on sustainability and responsible mining through Environmental, Social, Governance, and Sustainability-related matters.

We invite you to share your knowledge and experience with an audience of like-minded individuals to inspire growth and change.

ENVIRONMENTAL

SOCIAL

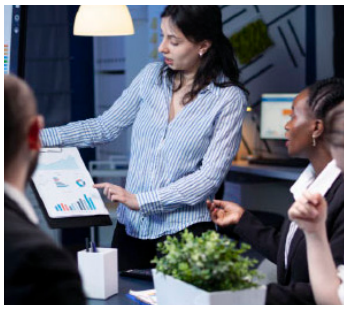

GOVERNANCE

SUSTAINABILITY

FOR FURTHER INFORMATION CONTACT:
Camielah Jardine: Head of Conferences and Events
E-mail: camielah@saimm.co.za
Web: www.saimm.co.za
Tel: +27 11 538 0237